Polymer/Carbon Nanotube Based Nanocomposites for Photovoltaic Application: Functionalization, Structural, and Optical Properties

Boubaker Zaidi [1,2,*], Nejmeddine Smida [3,4], Mohammed G. Althobaiti [5], Atheer G. Aldajani [1] and Saif D. Almdhaibri [1]

1   Department of Physics, College of Science and Humanities, Shaqra University, Dawadmi 11911, Saudi Arabia; s442481193@std.su.edu.sa (A.G.A.); s442500416@std.su.edu.sa (S.D.A.)
2   Laboratoire de Synthèse Asymétrique et Ingénierie Moléculaire de Matériaux Organiques Pour L'électronique Organique LR 18ES19, Department of Physics, Faculty of Science, University of Monastir, Monastir 5019, Tunisia
3   Department of Chemistry, College of Science and Humanities, Shaqra University, AlQuwaiiyah 19257, Saudi Arabia; nejm.smida@su.edu.sa
4   Laboratory of Interfaces and Advanced Materials, Faculty of Science, University of Monastir, Monastir 5019, Tunisia
5   Department of Physics, Faculty of Science, Taif University, Taif 21974, Saudi Arabia; m.althobaiti@tu.edu.sa
*   Correspondence: boubaker@su.edu.sa

Abstract: We present a systematic review of nanostructured organic materials, including synthesis methods, functionalization, and applications. First, we report the chemical and physical procedures used for preparing the polymer/carbon nanotube composites described in the literature over the last decade. We compare the properties of different polymer-based prototypes of organic nanocomposites functionalized with carbon nanotubes. Theoretical and experimental vibrational investigations provide evidence of the molecular structure describing the interaction between both components, showing that the allowed amount of carbon nanotubes and their dispersion states differ across polymers. Moreover, the nature of the solvent used in the preparation has a significant impact on the dispersion process. The integration of these materials in photovoltaic applications is discussed, where the impact of nanoparticles is evidenced through the correlation between experimental analyses and theoretical approaches based on density functional theory. Alterations in optical properties, evaluated from the absorption and luminescence process, are coherent with the solar spectrum, and a good distribution of donor/acceptor interpenetration was observed. In all cases, it was demonstrated that the performance improvement is physically related to the charge transfer from the organic matrix to the nanoparticles.

Keywords: PVK; hexylthiophene; PANI; nanocomposite; photovoltaic cells; DFT

1. Introduction

Scientific communities are continuously exploring innovative properties of π-conjugated conducting polymers, used as active layers in various organic electronic devices [1–4]. Hence, diverse molecular engineering procedures have been reported, such as doping conjugated polymers with conductive elements to ameliorate their conductivities [5,6]. Compared to inorganic semiconductors, these materials offer good flexibility and easier processing, leading to easier modulation of electronic, optical, and mechanical properties [7–13]. Handicaps related to fragility and a lower operating lifetime can be overcome by adding a small amount of carbon nanotubes (CNTs) [14,15]. Recently, Subramanyam et al. demonstrated that the addition of CNTs helps achieve an increase in lifetime by 67% in an open atmosphere [16]. According to Francis et al., CNTs also improve charge transport and provide good thermal stability, allowing π-conjugated conducting polymers to be good

candidates for electrical, thermal, sensing, and actuating applications [17]. If CNTs are well dispersed and the exciton diffusion length is sufficient, the configuration leads to charge and energy transfer in the organic matrix [18–20]. This transfer is a major parameter for good photovoltaic conversion. Hence, the separation process of electron–hole pairs should dominate if the diffusion length is sufficiently higher than the mean distances between nanoparticles. The resulting interpenetrating (bulk P–N hetero-nanojunctions) network results in a good overlap between the optical absorption (OA) spectral region and the solar spectrum [21]. Indeed, the decrease in the optical gap involves additional absorption features in the visible spectrum and leads to a higher charge separation and good collection efficiencies [22–25]. Hybrid materials, including inexpensive flexible polymers and their nanostructures, represent the next generation of photovoltaic solar cells [26]. Continuous progress in and improvement of fabrication methods is a major focus of research [27]. The aim is to ensure a uniform distribution and arrangement of nanoparticles in the polymer matrix. The performance of organic photovoltaic solar cells is comparable to that of monocrystalline silicon, where PCE reaches 24% [16].

CNTs exist in a bundled form in the solid state. The dispersion process requires mechanical or vibrational energy higher than van der Waals cohesive forces [28]. The direct mixing methods are based on mechanical agitation or vibrational forces using homogenizers with different velocities [29,30]. CNTs with better homogeneity and alignment can be achieved by applying to the nanocomposite an ultrasound wave and centrifugal forces of appropriate power for an appropriate amount of time [31,32]. Chemical or physical functionalization, through covalent or noncovalent bonding between CNTs and diverse active molecules, has also been reported [33,34]. For chemical functionalization of the CNT surface (Scheme 1a,b), the bonding can be via defect groups or by side wall bonding, as well as by other special reactive groups, such as lithium alkyl nitrenes and fluorine radicals [35–37]. These chemical modifications facilitate the grafting of other functional groups and give rise to covalent bonding with the polymers/molecules [38]. However, noncovalent functionalization can be hexahedral (Scheme 1c,d) or endohedral [39].
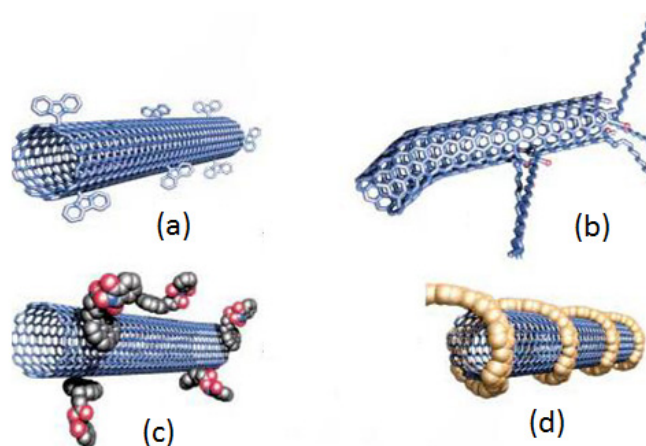
Scheme 1. Interaction between CNTs and functional molecules covalently (**a,b**) and noncovalently (**c,d**) [39].

For a polymer moiety, the polymerization process can be carried out after chemical functionalization, where first the monomers are linked to the tube and then the polymerization takes place [40,41]. If the direct mixing of polymers or in situ polymerized fragments with CNTs results in noncovalent linking, the process is called physical functionalization (Scheme 2) [42–46].
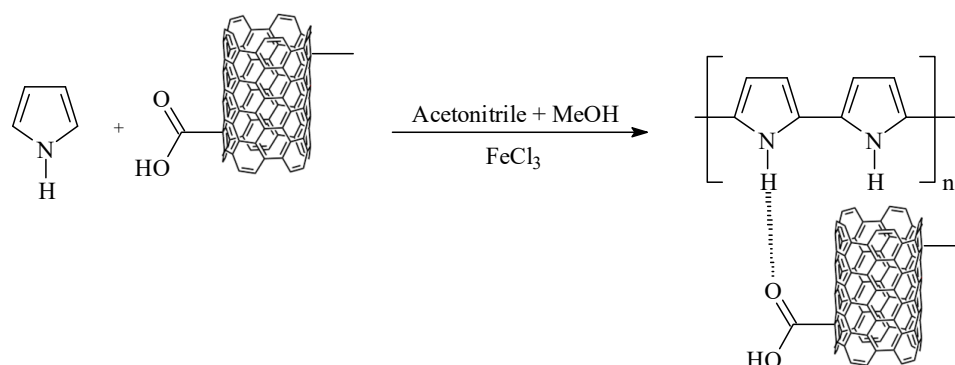
Scheme 2. Interaction between polypyrrole and multiwalled CNTs.

The dispersion process of nanoparticles is often of short duration. These nanoparticles have the tendency to agglomerate on the surface. To separate aggregates, the obtained solution should be exposed to ultrasonic baths and centrifuge forces with controlled frequencies and power [47]. In this work, we present various methods used over the last two decades for nanocomposite elaboration for a specific class of polymeric materials and their impact on the amelioration of photovoltaic properties. The study is restricted to polymer materials containing nitrogen in the aliphatic or cyclic sequences, such as poly(N-vinyl-carbazole) (PVK), poly(3-hexylthiophene (P3HT), and polyaniline (PANI). We report the results of our investigations in the last decade of the different polymeric nanostructures based on a large variety of polymers. As indicated for nanostructured materials, photoexcitations are followed by the establishment of charge transfer. The electronic structure modification, including the highest occupied molecular orbital (HOMO) and the lowest unoccupied molecular orbital (LUMO) levels, localized states, their energies, and the corresponding skin depth, should be evaluated in order to reduce injection barriers. Density functional theory (DFT) calculations are additional alternatives applied to a justified model structure to support experimental characterizations and physical interpretations [48–53]. Properties of organic materials that are experimentally inaccessible are in general described by DFT-based quantum calculations [50,53,54].

2. Organic Nanocomposite Synthesis and Characterization

2.1. CNT Treatment and Dispersion

CNTs (single-walled or multiwalled forms) need some treatment before functionalization with organic materials. Purification can be ensured either chemically, using a selective oxidation processor, or physically, based on filtration and/or centrifugation [55–58]. Metallic and semiconducting nanotubes can be separated by gradient-of-density ultracentrifugation techniques. The difference in their diameters is also exploited in the separation process [59,60]. Selective interaction with a conducting polymer is an alternative procedure that is efficient for separation in an acidic medium [61].

Good dispersion (homogeneous distribution) of CNTs in the polymer matrix is a major step that influences their properties [62]. CNTs largely exist in the bundled form due to strong van der Waals cohesive forces. It is difficult to achieve the isolated form, and the functionalization process leads to aggregate formation (Figure 1). Concerning the composite preparation, purified single-walled carbon nanotubes (SWCNTs) are dispersed in the same solvent with a polymer for an appropriate amount of time. The transitory dispersed phase of SWCNTs is immediately added in the desired amount to the polymer solution. Then, the sonication process and centrifuge forces are applied.
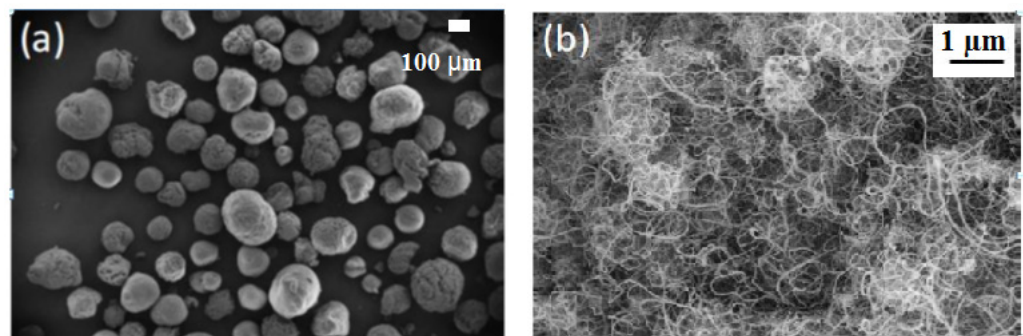
Figure 1. Structure of the bundled CNT (**a**); a zoom-in photo of the aggregates (**b**).

2.2. Materials and Methods

Composite solutions were deposited at room temperature with nearly uniform thickness on silica substrates for OA measurements. However, glass slides were used for FTIR and photoluminescence (PL) measurements. All substrates were already cleaned with deionized water and ethanol in an ultrasonic bath. All samples thus obtained were introduced into a Pyrex tube and heated under vacuum at a moderate temperature based on the thermal stability of the resulting material. Infrared absorption measurements were recorded with a resolution of 2 cm^{-1}. The OA spectra were recorded in the absorption mode with the wavelength varying from 200 to 2000 nm. For the PL experiment, depending on the material emission spectral range, different excitation wavelengths were used (280, 325, and 540 nm). Ultrafast time-resolved PL measurements were carried out with the regenerative amplified femtosecond laser system. The time-resolved emission spectra were spatiotemporally detected with a high-dynamic-range Hamamatsu C7700 streak camera with a temporal resolution <20 ps. The PL intensity and decay times were simulated with two coupled exponential decays. The TEM images were observed after adding liquid nitrogen to the Cu grid and then were taken at temperatures varying from 100 to 104 K. Theoretical data were procured from quantum calculations based on density functional theory (DFT). The modeling structure was fully optimized using the most popular Becke's three-parameter hybrid functional, B$_3$ [63], with the basis set 6-31G(d). Calculations applying to the proposed modeling structures were carried out with nonlocal correlation of Lee–Yang–Parr (LYP), abbreviated as the B$_3$LYP method. Theoretical OA spectra were calculated using the time-dependent density functional theory (TD-DFT) method with the 6-31G(d) basis.

2.3. Alignment and Orientation of CNTs

CNT orientation can be accomplished in solution during or after the polymer synthesis process. Chemical vapor deposition synthesis of SWCNTs results in a massive growth of superdense and vertically aligned nanotubes with enhanced catalytic activity of catalysts (Figure 2) [64]. CNTs can also be aligned under a magnetic or an electric field during the growth step, but some dynamic structural changes can occur due to the complexity of the process [65–68].
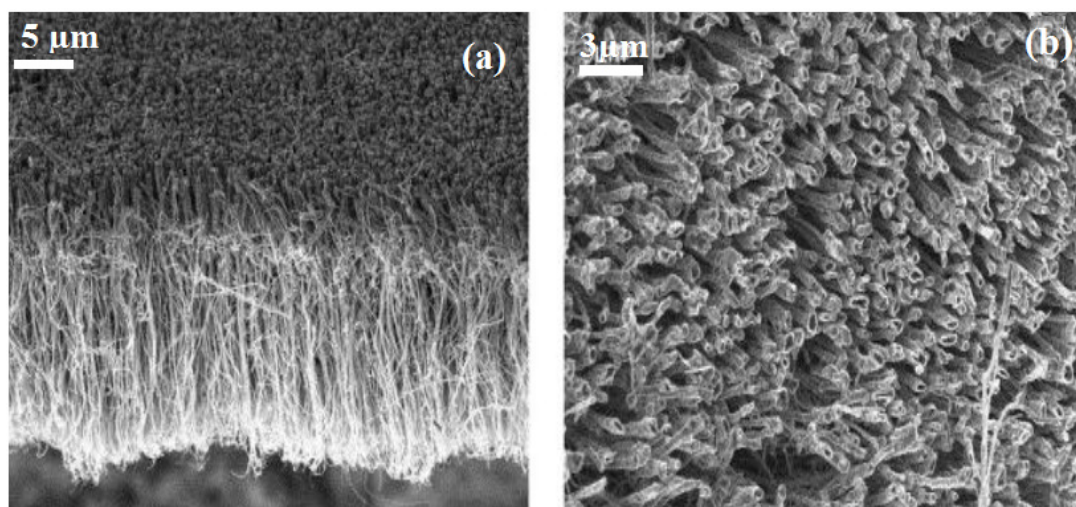
Figure 2. TEM pictures illustrating CNT orientation observed in (**a**) the lateral direction and (**b**) the longitudinal direction [69].

After CNT dispersion, the application of external electrical or magnetic perturbations allows the orientation of CNTs in the preferred direction [70–75]. This network formation results in three steps: the orientation of nanotubes, interaction, and network establishment (Scheme 3). Due to dipolar interaction, the aligned CNT configuration leads to tail-to-tail or head-to-head connections.
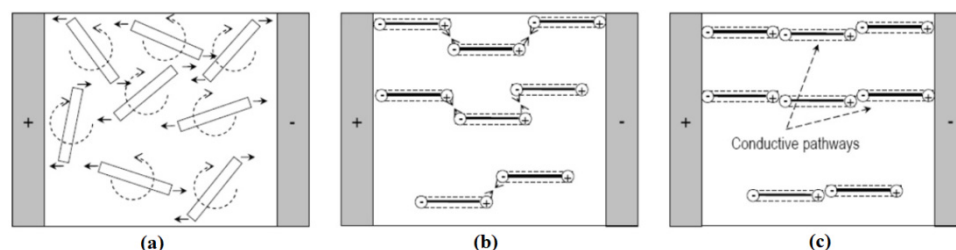
Scheme 3. Network formation: (**a**) orientation, (**b**) interaction between oriented CNTs, and (**c**) the resultant network [76].

In both cases, the oriented CNTs permit the reinforcing of optical and electronic transport properties in the preferred direction. This process helps enhance the performances of the electronic and optical devices. Moreover, annealing at moderate temperatures leads to a good repartition of CNTs into the organic polymeric matrix, which results in higher photovoltaic performances [77–79].

3. Applications of Organic Nanocomposites for Photovoltaic Cells

Organic solar cells represent new alternatives to those based on inorganic semi-conductors [16]. Organic materials are characterized by flexibility, lightness, low cost, and easy processing. However, their intrinsic charge carrier mobility is lower (at max 10^{-1} cm^2 V^{-1} s^{-1}) compared to that of their homolog inorganic semiconductors, where it can reach 900 cm^2 V^{-1} s^{-1} for a single silicon crystal. Otherwise, handicaps related to lower mobility and fragility can be partially resolved when adding CNTs or phenyl C61 butyric acid methyl ester (PCBM) because carbon structures exhibit better mobility and rigidity than silicon [80]. Therefore, adding a small quantity of CNTs (single-walled or multiwalled forms) may improve the mechanical properties and lead to a good compatibility with the solar spectrum (UV–visible range). If, additionally, there is coherence between diffusion length (~20 nm) and the distances between CNTs, the separation process of electron–hole pairs will be improved. In fact, when adding CNTs, the entire network will be regular nano-P–N junctions, which represent photogeneration sites in all points. The

charges transferred from the organic matrix to CNTs may be simultaneously collected and carried by CNTs. In the literature, the open-circuit current for some elaborate photovoltaic devices is in the range of a few tens of milliamperes per square centimeter [81–84]. This nanometric configuration is different from the conventional inorganic P–N photovoltaic cell. Indeed, for an inorganic device, a single junction separates the P and N regions, while in the nanometric interpenetrating network, junctions are distributed in the entire bulk, giving rise to more photoexcitations, leading to higher efficiency.

For organic photovoltaic conversion, efficiency started with values lower than 1%. However, the conversion efficiency was considerably improved beginning from the year 2000, reaching 2.5% and then 3.6% when PCBM was inserted in the organic matrix [85,86]. The relatively high conversion efficiency is obtained with a double heterostructure of fullerene (C_{60}) and copper phthalocyanine [87]. In 2011, a new record of 5% was attained using hybrid CNT/polymer materials and then ameliorated to reach 12% [10]. Compared to a silicon monocrystal, the power conversion efficiency (PCE) remains lower, but the easy processing and low cost make the material attractive [10]. The actual records were achieved by Cui et al. in 2020 and Subramanyam et al. in 2021, reaching, respectively, 17% and 24%, comparable to the PCE of porous and crystalline silicon [16,88].

4. Nanocomposites of Oligo-N-vinyl-carbazole/Single- and Multiwalled CNTs

Infrared, Raman, OA, and PL spectroscopies were used to describe the interaction between OVK and SWCNTs in polar and apolar solvents. The effect of the solvents' polarities on the dispersion process, i.e., repartition of SWCNTs on the organic matrix and its relationship with optical and vibrational properties, is reported. The observed changes in characteristics and their interpretations are discussed according to the literature [89–92]. Experimental results are correlated to those theoretically obtained from DFT; the functional and the method are described elsewhere [63,93–95].

4.1. Vibrational Properties

OVK/SWCNT composites were prepared at various concentrations in different solvents, such as chloroform and chlorobenzene, and were annealed to ameliorate the dispersion process [21,96]. FTIR spectra depicted in Figure 3 reveal that the most relevant vibrational modes of native OVK and SWCNTs are found in the composite spectrum. Moreover, in both cases, adding SWCNTs leads to some significant changes. Some bands with a relatively higher intensity ascribed to OVK vinyl groups disappear, which is strictly related to the linking between SWCNTs and OVK. This grafting is spontaneously established in the case of chloroform. However, when dispersing in chlorobenzene, certain spectra can be recorded after annealing treatment at 393 K (as in the case of nanocomposite dispersed in chloroform). Indeed, a better modification of the spectrum is clearly seen after annealing, and both spectra (a) and (c) present higher similarity. In both cases, the spectra reveal the appearance of a new feature at 1297 cm^{-1} that indicates the covalent interaction between organic OVK matrix and CNTs, as described for electrosynthesized PVK/SWCNTs [97].

Raman analyses (Figure 3(2)) reveal the presence of SWCNT bands, but those of OVK are severely attenuated. Radial and tangential modes depend on the used solvents and thermal treatment, which reflect the dispersion state of CNTs in the organic matrix (decrease in the band attributed to the bundled form at 181 cm^{-1}).
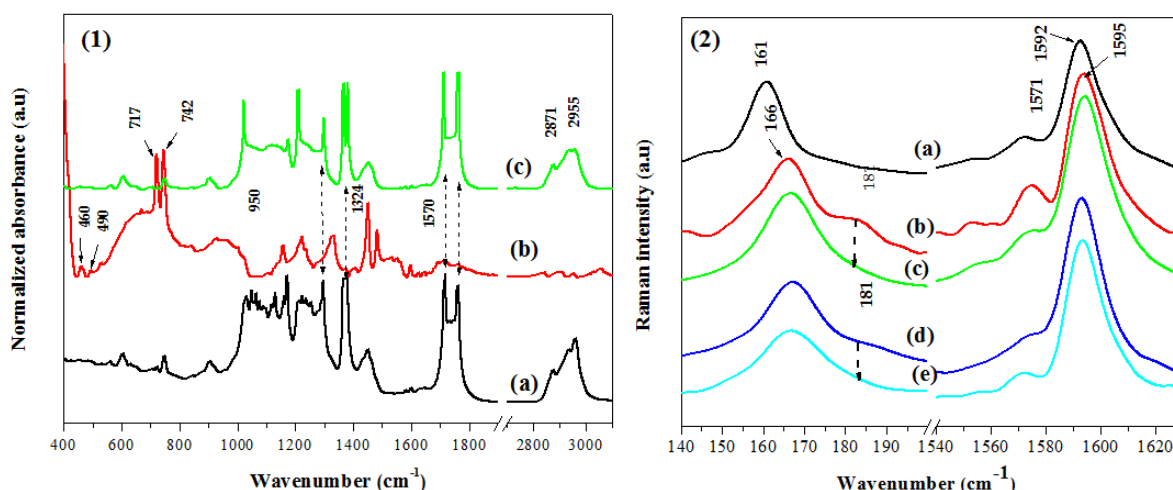
Figure 3. (**1**) Infrared spectra of the OVK/SWCNT composite dispersed in a chloroform solvent (**a**) and a chlorobenzene solvent (**b**) not annealed and (**c**) annealed at 333 K. (**2**) Raman radial and tangential modes: (**a**) SWCNTs; OVK/SWCNT in chloroform in the not-annealed (**b**) and annealed (**c**) states; OVK/SWCNT in chlorobenzene in the not-annealed (**d**) and annealed (**e**) states.

Both radial mode bands at 161 and 181 cm^{-1} are associated, respectively, with isolated and bundled SWCNTs [98,99]. The mean diameter of the tube can be evaluated from the empirical relation and varies from 1.34 to 1.38 nm [96,100]. The shift in radial mode toward higher wavenumbers has been interpreted as a consequence of inserting organic molecules into bundled SWCNTs. The disappearance of radial mode (bundled CNTs) in the case of the chlorobenzene solvent leads to the conclusion that the polar solvent leads to more dispersed nanotubes. The change from 2D to 3D symmetry is illustrated by the tangential mode narrowing and the decrease in intensity for the mode at 1571 cm^{-1} [101]. The spectrum of annealed states reveals shifting and band intensity modifications, promoting a better functionalization process.

4.2. Changes in Optical Properties

The most relevant information on the excitation and de-excitation process can be described by the complementarity of OA and PL measurements (Figure 4).
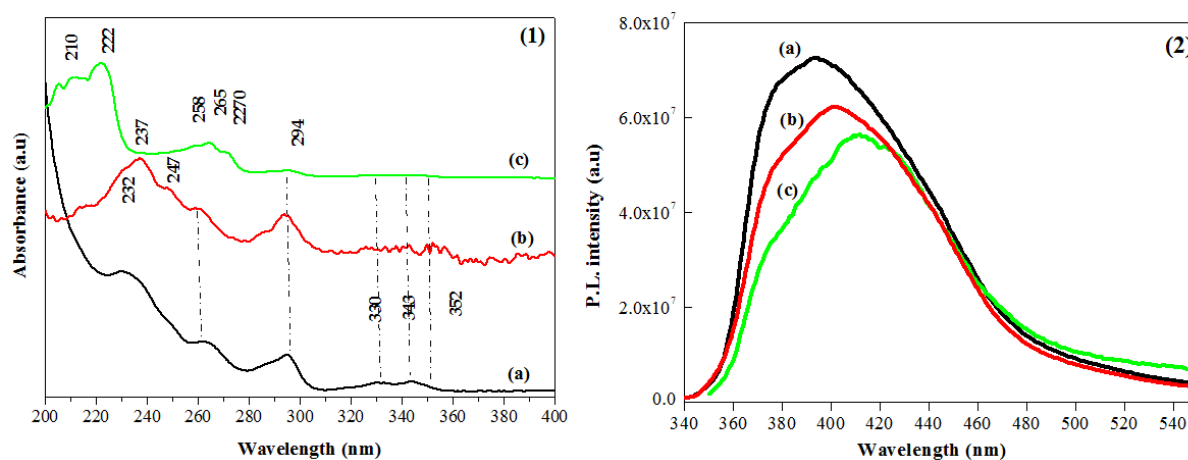
Figure 4. Changes in OA (**1**) and PL (**2**) spectra. Before SWCNT addition (**a**) and after SWCNT addition in chloroform (**b**) and in chlorobenzene (**c**).

Absorption spectra are affected by adding SWCNTs. For both solvents (chloroform and chlorobenzene), we see a redshift and a new band apparition, implying an interaction

between both components. When chloroform is the solvent, in the spectral region of 400 to 2000 nm, there is a gradual decrease in the absorbance, similar to the case of other polymers when functionalized with SWCNTs [21,102]. Bands that appear in this spectral region (λ > 400 nm) correspond to the optical transitions for semiconducting SWCNTs. In chlorobenzene, the hypsochromic shift of the blue-side transition implies a decrease in the oligomer chain length and/or a decrease in the interchain interaction due to the good dispersion of SWCNTs in the organic matrix [81].

Chlorobenzene as a solvent quenches PL intensity after SWCNT insertion more efficiently (Figure 4(2)). This result is in good agreement with Raman results supporting good SWCNT dispersion. Indeed, photoexcitations are followed by a separation process rather than a recombination, because of which the observed PL is quenched [89,103,104]. We think that the photoexcitation produced in the OVK matrix can reach SWCNTs where the dissociation process is more preponderant rather than the recombination process. After annealing, the quenching effect becomes more pronounced and a new feature emission is created at around 499 nm (2.48 eV) when chloroform is the solvent (Figure 5(1)). As at a lower temperature (T = 87 K) and for both annealed samples (with and without SWCNTs), this weak emission band appears only in the case of the composite. It is, therefore, the consequence of the insertion of SWCNTs (Figure 5(2)).
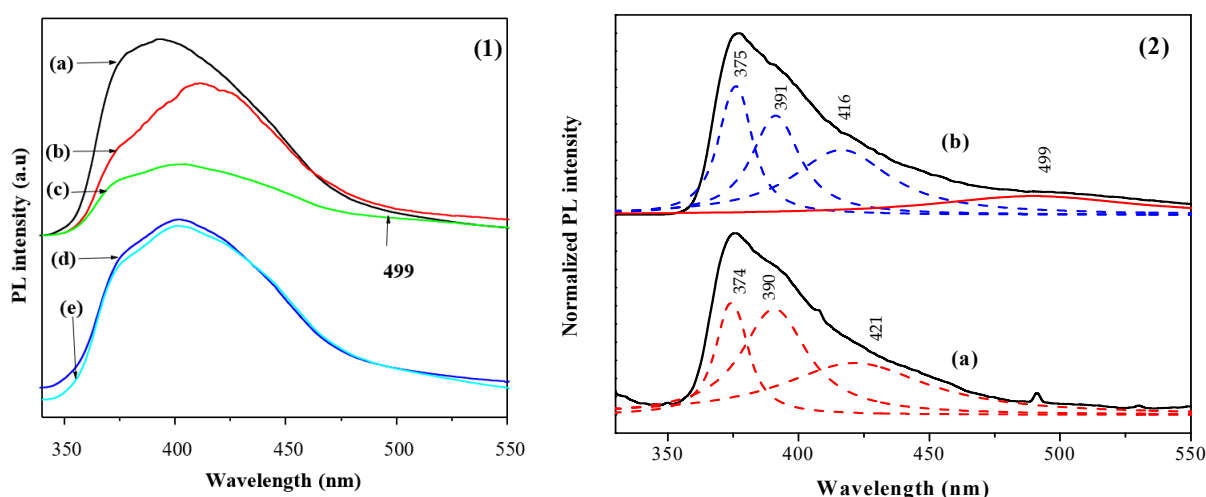
Figure 5. (**1**) Stationary PL spectra of (**a**) OVK and of nanocomposite in chloroform (**b**) not annealed and (**c**) annealed at 333 K and in chlorobenzene (**d**) not annealed and (**e**) annealed at 333 K. (**2**) PL spectra at T = 87 K of both annealed samples (**a**) OVK and with the OVK/SWCNT composite (**b**).

4.3. Interaction between SWCNTs and an Organic Matrix

The correlation of experimental and theoretical results evidences the covalent functionalization process between SWCNTs and oligo-N-vinyl carbazole [21]. The process does not require any thermal treatment when the dispersion is in chloroform as the solvent. The most affected chemical environments are vinylidene groups because, we assume, grafting occurs between these groups and the side wall (Scheme 4), similar to the case of PVK/MWCNT and for PVK/C60 composites [98,101]. However, after annealing, the similarity of both spectra supports the same grafting process.

Scheme 4. Grafting mechanism of OVK and CNTs.

The proposed grafting mechanism, confirmed in our previous work, is consolidated by theoretical vibrational frequencies obtained either for OVK or for OVK/SWCNT composites [21]. First, experimental results are reproduced to confirm the modeling structures of primary materials. Then, the most probable grafting sites with higher reactivity are supported by force constant calculations in both neutral and oxidized states. In the resulting model structure of the nanocomposite, therefore, OVK is grafted on the side walls via vinylidene groups (Figure 6(1)).

Figure 6. (**1**) Nanocomposite modeling structure used for DFT calculation and (**2**) change in the electronic structure from OVK (**a**) to the nanocomposite (**b**). H: HOMO; L: LUMO; Exp: experimental.

Based on the above modeling structure, DFT has also been calculated with the B3LYP/3-21G* method to carry out changes in the electronic structure. All the theoretical changes are depicted in Figure 6(2), which are in good accordance with experimental absorption transitions.

4.4. Structural Properties in Relationship with Transient Photoluminescence

Transmission electron microscope analyses were carried out to have an idea about the SWCNT distribution and arrangement (Figure 7) [18].
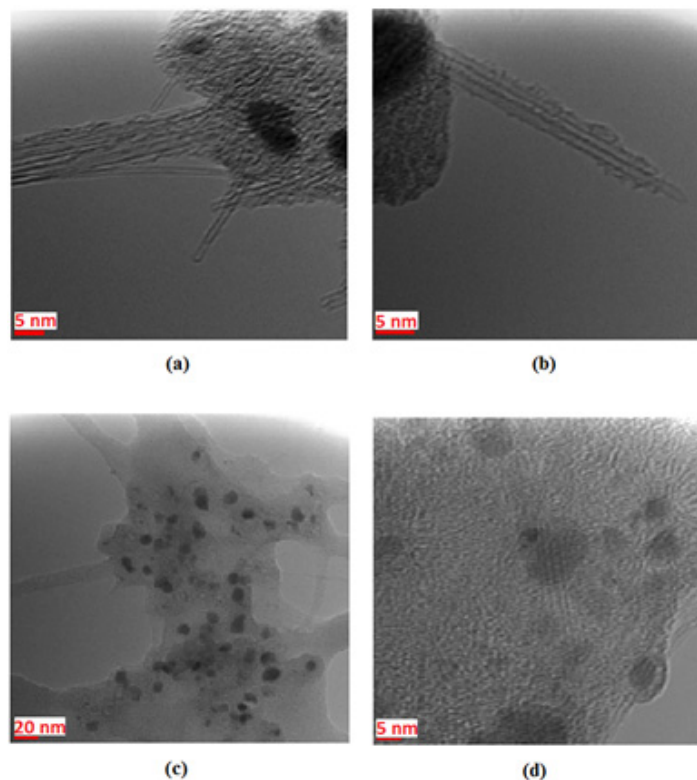
Figure 7. TEM pictures of OVK/SWCNT composites dispersed in chloroform (**a**,**b**) and in chlorobenzene (**c**,**d**) [18].

When chloroform is the solvent, bundled and isolated SWCNTs are detected, but with a lower concentration for the isolated form, supporting a good SWCNT dispersion process. Figure 7c shows a good uniformity and orientation of SWCNTs having an interdistance of nearly 10 nm, probably due to the thermal treatment. In chlorobenzene (Figure 7d), this distance varies from 3 to 20 nm and the structure contains bundled SWCNTs connected by individual ones. In fact, these structural differences can influence the dynamical properties of the excited states.

Results of PL decay (obtained by pumping at 330 and probing at 390 nm) show a decrease in lifetimes and imply exciton diffusion to the SWCNTs [18,105,106] (Table 1).

Table 1. Decay parameters of OVK/SWCNT nanocomposites [18].

Samples	P_1 (%)	P_2 (%)	τ_1 (ns)	τ_2 (ns)	A_1	A_2	τ_m (ns)
OVK	18.8	81.10	0.983	6.223	8.911	6.042	5.23
OVK/SWCNTs in chloroform	32.73	67.26	0.753	6.996	15.575	3.445	4.95
OVK/SWCNTs in chlorobenzene	32.98	67.01	0.662	3.848	13.747	4.804	2.796

The existence of two populations weighing P_1 and P_2, having lifetimes of τ_1 and τ_2, and having a mean lifetime τ_m has been interpreted to be because of shorter and longer segments, respectively. A similar decay evolution was reported in the case of other polymers functionalized with various nanoparticles [107,108], supporting a charge transfer between the organic matrix and SWCNTs [105,109]. Lifetimes evaluated from Figure 8(1) are shorter than those of PVK, which is coherent with the fact that faster decay is a signature

of shorter segments [110,111]. The photoexcitations that occur in the organic matrix will diffuse and be transferred into the SWCNTs, and the electron–hole pairs will be separated due to the internal electric field created by hetero-nanojunctions [81,83]. The obtained decay times are coherent with PL cartography (Figure 8(2)), in which we show a more intense luminescence when chlorobenzene is the solvent. Indeed, a faster lifetime results in the condensation of excitations in the radiative pathways.
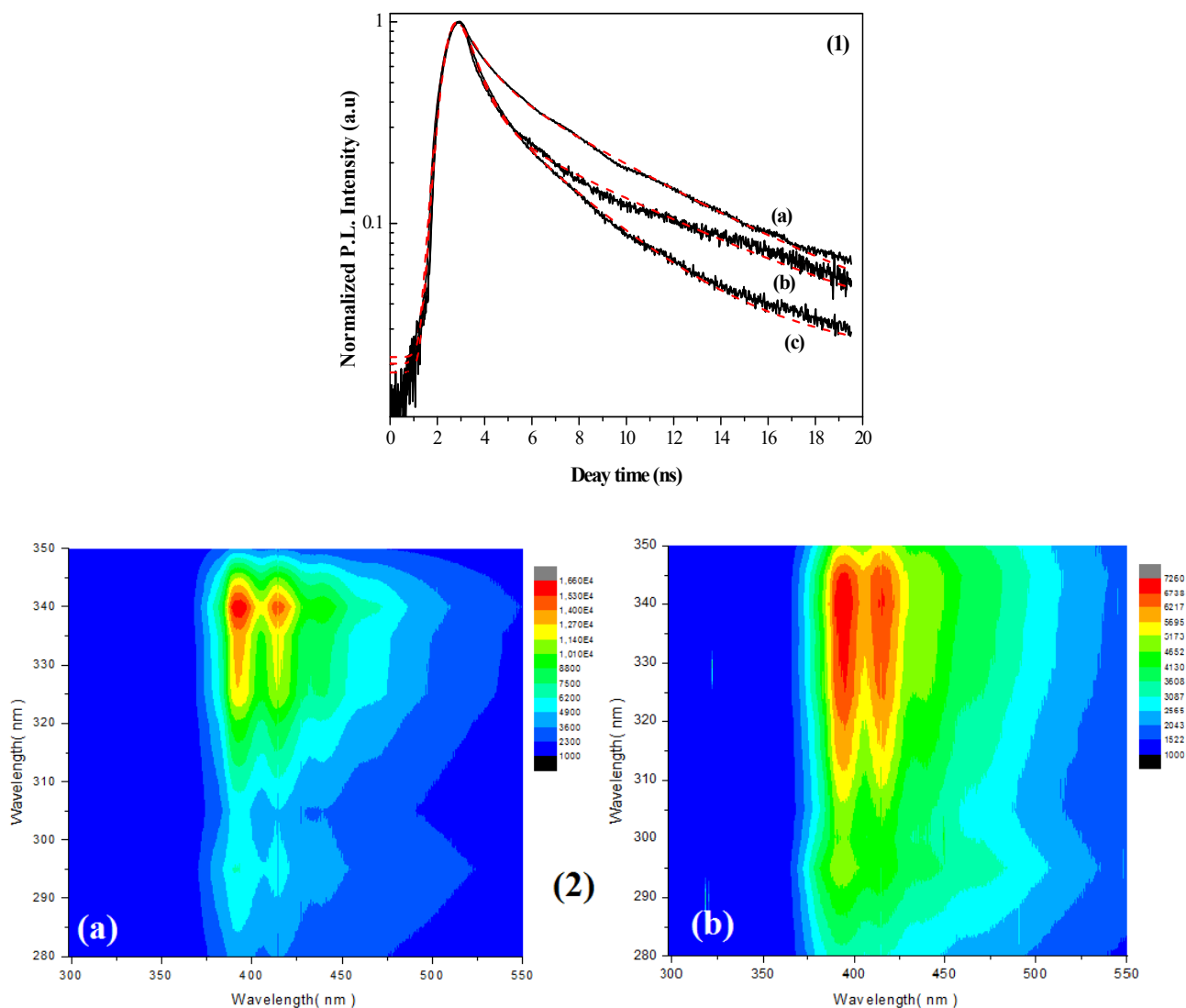
Figure 8. (**1**) PL decay OVK (**a**), OVK/SWCNTs in chloroform (**b**), and OVK/SWCNTs in chlorobenzene (**c**) (—: experimental; (. . . .): theoretical). (**2**) PL cartography of OVK/SWCNTs in chloroform (**a**) and in chlorobenzene (**b**).

5. Properties of PVK-3HT/SWCNT Nanocomposites

To reach a better dispersion process with a higher CNT concentration and to obtain good optical properties, another matrix containing PVK was synthetized [29,112]. Hexylthiophene, known by a large optical spectrum, was bridged with PVK, where the resulting matrix is called PVK-3HT. PVK-3HT/SWCNT nanocomposites were studied by FTIR and Raman spectroscopy, where the SWCNT weight concentration varied from 0% to 60%. It was shown that in all cases, SWCNTs are bundled and isolated. However, the D-band and the G-band, situated at 1250 and 1595 cm^{-1}, respectively, are nearly the same in all cases, similarly to the case of purified nanotubes.

5.1. Vibrational Study

On adding SWCNTs to PVK-3HT, there is no apparent change in the band positions and shapes of both compounds. However, the band intensities change and the appearance of new vibrational features at 1049 and 1384 cm^{-1} (Figure 9(2)) lead to the conclusion that there is an interaction between both components.
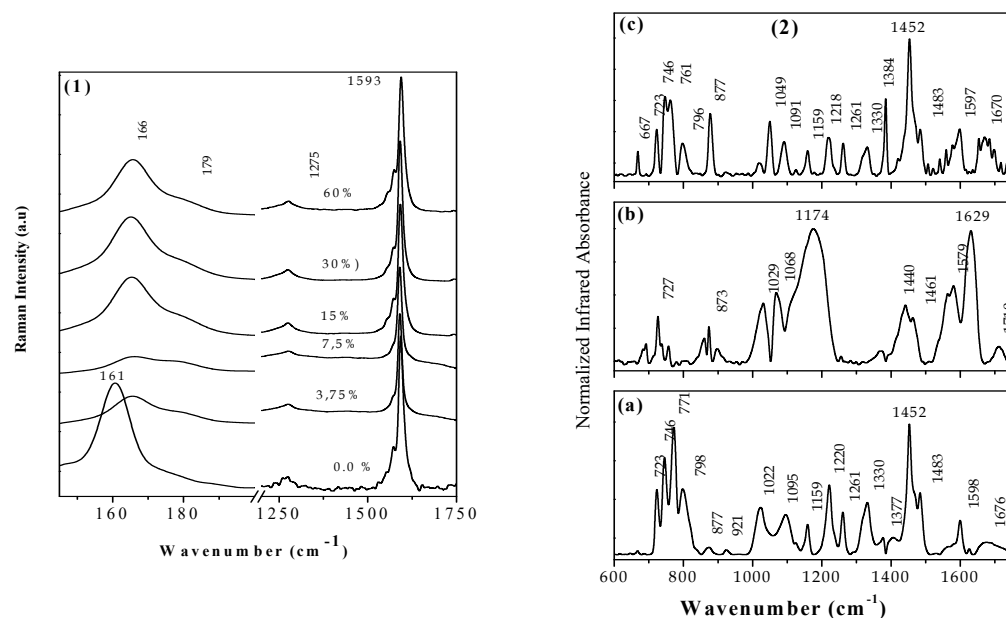
Figure 9. (**1**) Raman spectra of PVK-HT/SWCNTs at different CNT weight concentrations (0%, 3.75%, 7.5%, 15%, 30%, and 60%). (**2**) FTIR spectra of PVK-HT (**a**), SWCNTs (**b**), and PVK-HT/SWCNT composite (60%) (**c**).

5.2. Optical Properties Changes

UV–visible absorption analyses (Figure 10(1)) demonstrate that PVK-HT absorbs in the large spectral domain. The absorbance shape observed in the spectral domain ranging from 240 to 300 nm is the signature of the grafting of bicarbazole units as a part of the resulting copolymer [113]. The extension of the absorbance in the visible range indicates extended conjugated fragments of P3HT in the obtained copolymer [113,114]. On adding SWCNTs, no apparent change is observed for λ < 400. However, the band near 430 nm decreases and blue-shifts, which agrees well with the hypothesis of the diminution of interchain interaction and/or the decrease in the π-conjugation length [115].

The continuous PL quenching (Figure 10(2)) shows that the addition of CNTs has a direct impact on the excited-state dynamics of the prepared composite (exciting at 400 nm using a seep range of 1 ns) [111]. As in the case of the OVK/SWCNT composite, we think that the exciton diffusion length becomes progressively higher than the distance between neighboring nanotubes. In this case, the separation process is the most dominant behavior that can occur.

These results are in full accordance with the progressive decrease in emitted energy intensity as a function of time from 0 to 1 ns obtained in 3D maps (Figure 11).
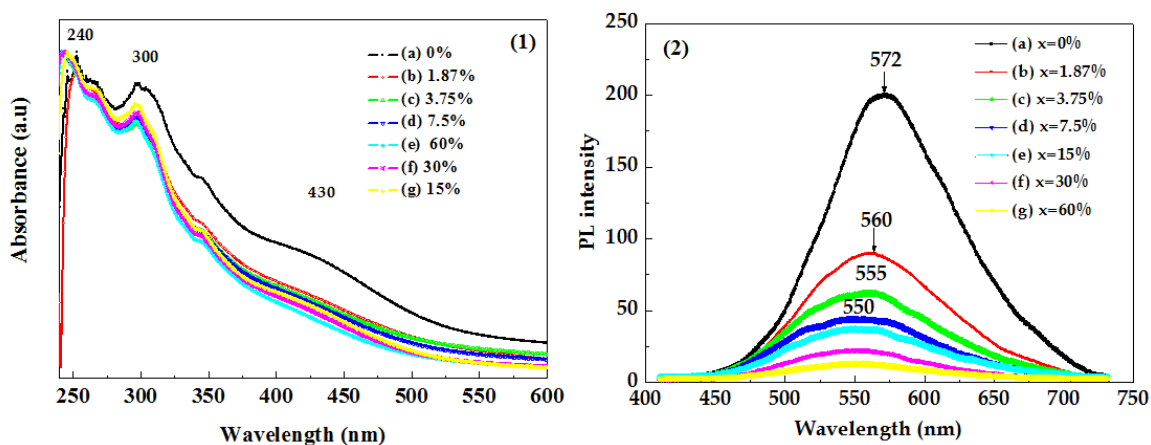
Figure 10. (**1**) OA and (**2**) PL spectra in chloroform solvent of pristine PVK-HeT (**a**) and those of PVK-HeT/SWCNT composites at various SWCNT weight concentrations: (**b**) 1.87%, (**c**) 3.75%, (**d**) 7.5%, (**e**) 15%, (**f**) 30%, and (**g**) 60%.
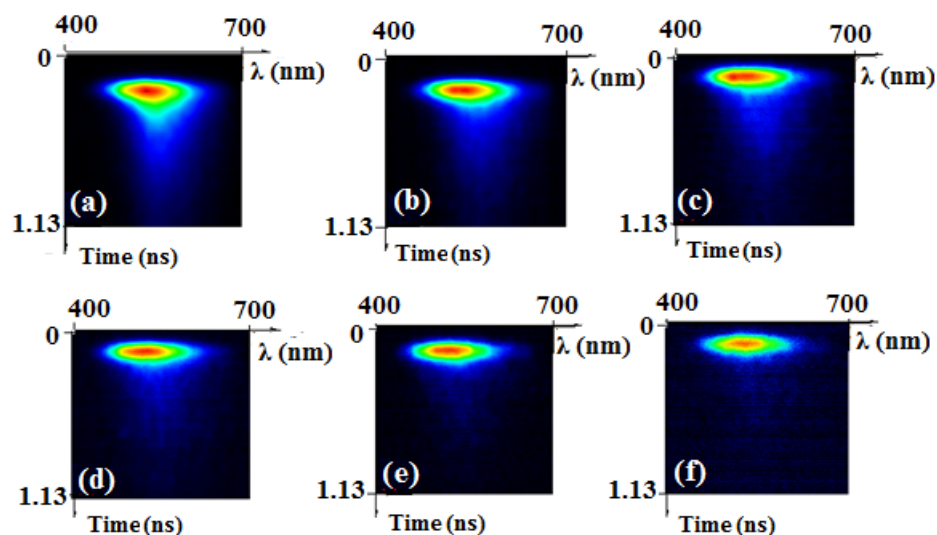
Figure 11. Contour plot of transient PL for PVK-HTs functionalized with different SWCNT concentrations: (**a**) 0%, (**b**) 1.87%, (**c**) 7.5%, (**d**) 15%, (**e**) 30%, and (**f**) 60%.

Time-resolved PL spectra are presented in Figure 12. A progressively faster decay time is obtained when increasing the SWCNT weight concentration, as in the case of the PPV/SWCNT composite [111]. This behavior confirms that SWCNTs play a role in charge separation after exciton diffusion. Indeed, a shorter lifetime is an indicator of the decrease in the distance traveled by the exciton. The increase in the SWCNT concentration will, therefore, progressively reduce these distances. If these distances become lower than the intrinsic diffusion length, charge transfer from the organic matrix to CNTs can occur. This transfer leads to a separation of electron–hole pairs rather than their recombination, because of which there is a progressive quenching of stationary PL.
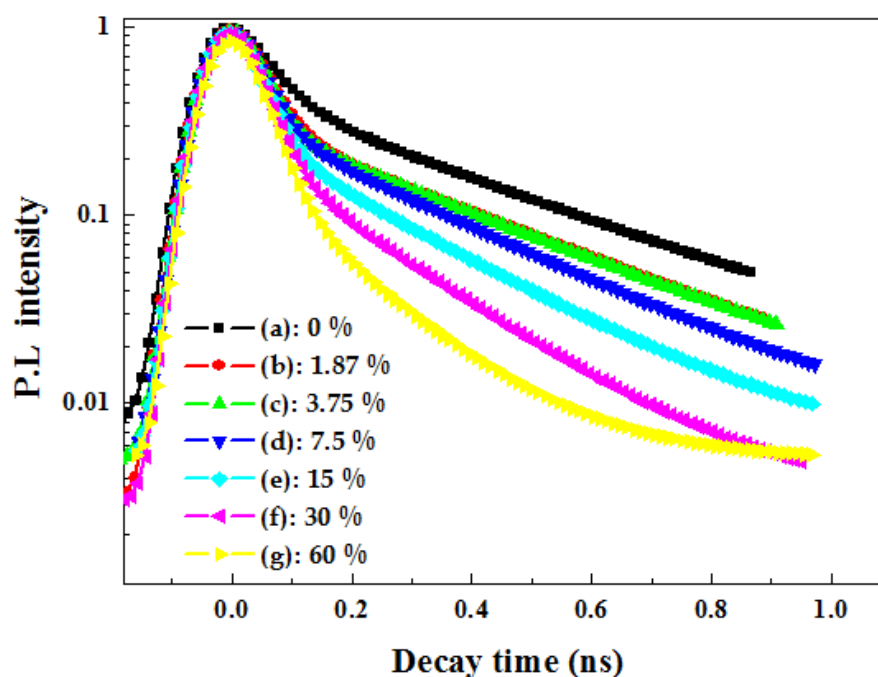
Figure 12. Time-resolved PL decays of PVK-HTs functionalized with SWCNTs at different concentrations: (**a**) 0%, (**b**) x = 1.87%, (**c**) 3.75%, (**d**) 7.5%, (**e**) 15%, (**f**) 30%, and (**g**) 60%.

6. PANI/SWCNT Nanocomposites

Following the same procedure, PANI, known by a number of oxidation degrees, is also functionalized with CNTs. The starting material, the emeraldine base (PANIEB purity 99.99%; macromolecular mass Mn > 15,000), is first doped with sulfonic acid and then functionalized with SWCNTs in the dimethylformamide (DMF) solvent [116]. The sulfonic acid doping procedure used in this case is described by MacDiarmid et al. [117].

6.1. Vibrational Study

The normalized FTIR spectra of Figure 13(1), when referring to the already published vibrational studies, reveal that concentrations lower than 2.10% cannot significantly induce apparent changes [118,119]. Starting from 2.1%, the linking of both components is evidenced by the appearance of new features at 1064, 1255, 1409, and 1438 cm^{-1}. Then, the apparent shift of both modes at 1124 and 619 cm^{-1}, the disappearance of the band at 1022 cm^{-1}, and the enhancement of bands in the range of 1350–1700 cm^{-1} reflect the new molecular arrangement induced by covalent bonding [120,121].

The weak band located at 1022 cm^{-1} ascribed to the C–H deformation disappears, and a new band appears at 1062 cm^{-1}. The bands situated in the range from 1350 to 1700 cm^{-1} show a better intensity increase, supporting the increase in aromaticity in the resulting compound. Two other new bands appear, one at 1409 cm^{-1} and one at 1438 cm^{-1}, and confirm covalent binding between both components via a C–N link [121].

A theoretical calculation including bond length, atomic charge, and spin density lead to the conclusion that nitrogen atoms are the most probable grafting sites, as in the case of similar woks [19,119]. In Figure 13(2), we illustrate the model structure that has been used for DFT calculation. Noncovalent bonding can also be present as a consequence of the strong van der Walls forces that inhibit the homogeneous dispersion process [122,123].
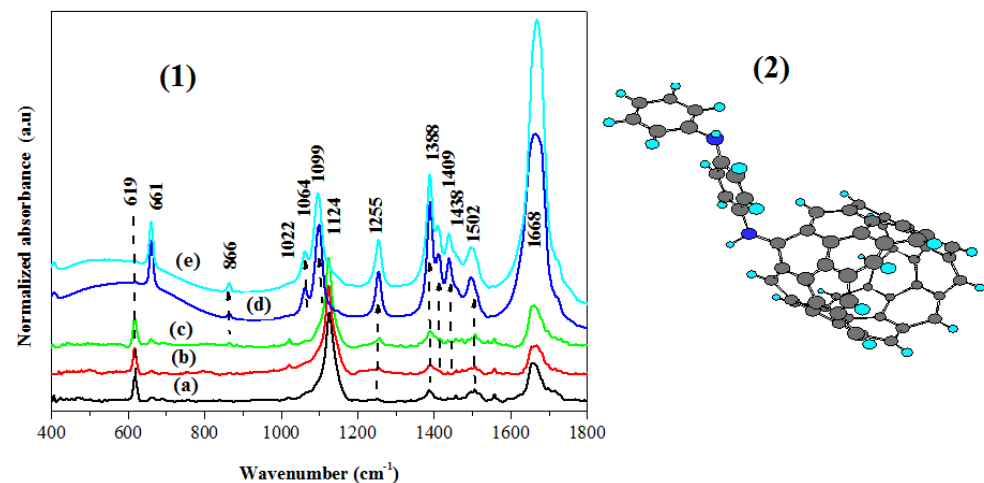
Figure 13. (**1**) FTIR spectra of PANI/SWCNT nanocomposites with various SWCNT concentrations: (**a**) 0%, (**b**) 0.71%, (**c**) 1.16%, (**d**) 2.10%, and (**e**) 5.00%. (**2**) Model structure of the nanocomposite used for DFT calculation [19].

6.2. Optical Property Changes

The modeling structure proposed above has been supported by theoretical calculation of OA spectra (Figure 14). The same transitions are found either experimentally or theoretically, for which it is noted that there is a diminution of band gap after either doping or adding SWCNTs. The energy gap of PANI in its neutral state is 3.75 eV; it decreases when doped and reaches 2.63 eV. A new band appears at −535 nm on adding SWCNTs, and the gap is 1.7 eV. This new band corresponds to the charge transfer where electron–hole pairs appear in the organic matrix, and then it is transferred to the SWCNTs by the diffusion process, leading to enhanced photovoltaic performances [18,96,124].
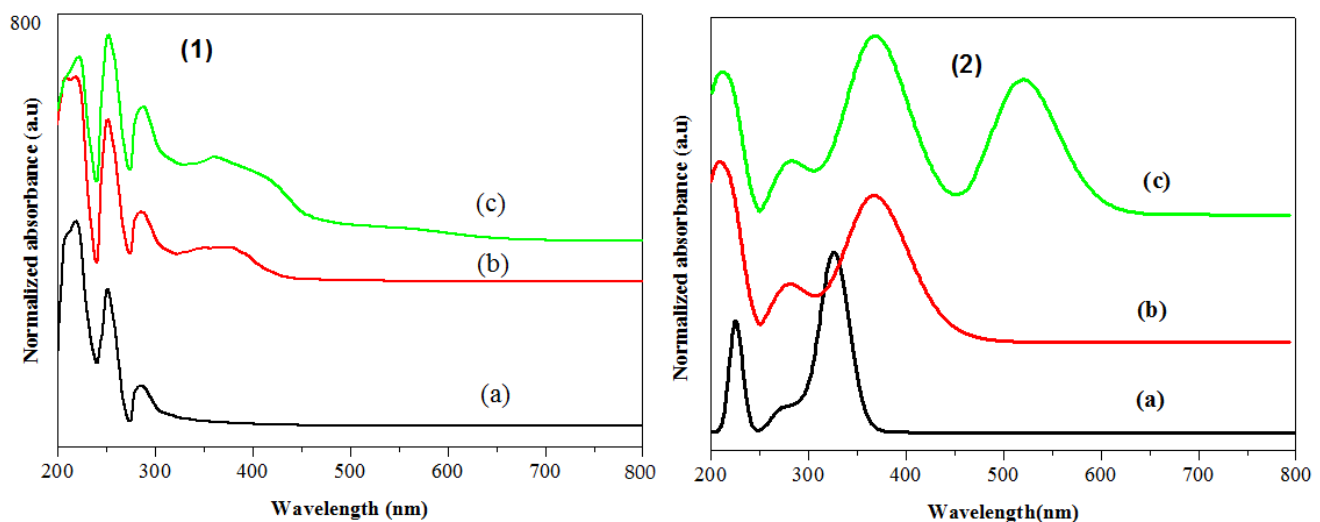
Figure 14. OA spectra of PANI in various states: (**1**) experimental and (**2**) theoretical; (**a**) neutral, (**b**) doped, and (**c**) the nanocomposite.

6.3. Electronic Study

The study on SWCNT concentration leads to the conclusion that localized states are created in the band gap with the energy of 1.62 eV and with the band width of almost 80 meV (Urbach energy) [121]. This donor–acceptor charge transfer is more elucidated by contour plots of molecular orbitals (MOs), shown in Figure 15(1) [125]. HOMO and LUMO state densities are, respectively, localized on donor and acceptor moieties [126].
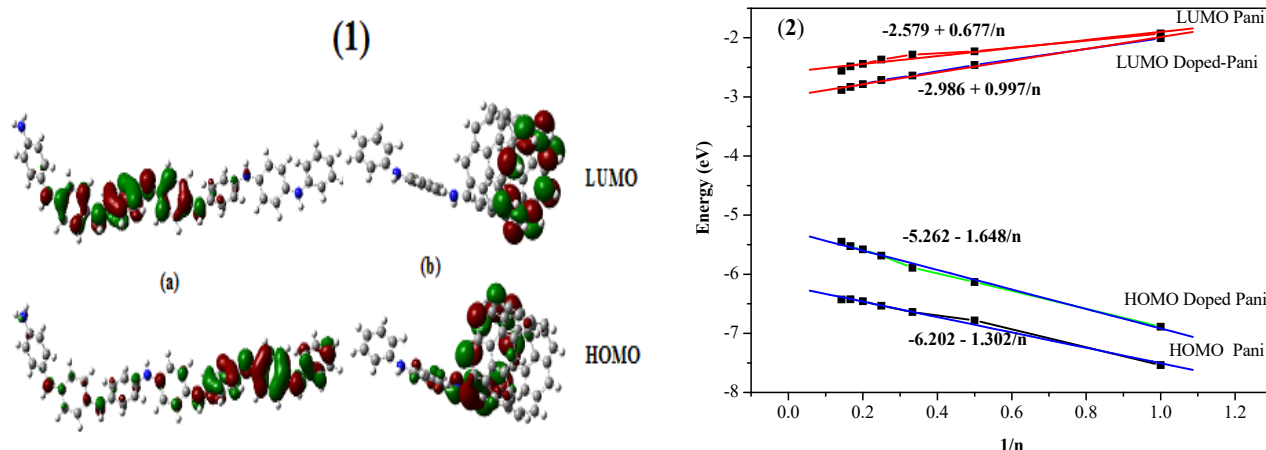
Figure 15. (**1**) HOMO and LUMO orbitals: doped PANI (**a**) and nanocomposite (**b**). (**2**) Effect of chain length on the HOMO–LUMO energy levels of PANI in pristine and doped states.

The ability of the resulting material to improve photovoltaic conversion is checked from its electronic structure (Figure 15(2)). Indeed, HOMO–LUMO energy levels are calculated from the optimization of model structures of pristine and doped states for different chain lengths [127].

The HOMO–LUMO energy levels for an infinite chain length can, therefore, be evidenced following Aleman et al. [127], where the theoretical energy gaps are 3.58 and 2.31 eV, respectively, for neutral and doped states. Other parameters can be evaluated, such as the PCE and the open-circuit voltage (V_{OC}). From the individual theoretical electronic structures (donor and acceptor), PCE can be evaluated using the Scharber diagram. Otherwise, the V_{OC} can be calculated according to Equation (1) based on the HOMO and LUMO energy levels of, respectively, donor and acceptor materials [128–131]:

$$V_{OC}(V) = \frac{1}{e}\left|E(HOMO)^{donor}(eV)\right| - \left|E(LUMO)^{acceptor}(eV)\right| - 0.3\,(V) \tag{1}$$

The choice of metal electrode is strictly based on the values of HOMO and LUMO energy levels for doped PANI and CNTs. It is found that Al and ITO are the most appropriate for the device architecture (Figure 16(1)). Using Equation (1), the V_{oc} is estimated at nearly 1.25 V, and using the Scharber diagram, PCE is estimated at 4–5% (Figure 16(2)). This is in good accordance with our previous PL results showing both the quenching effect and the total absence of luminescence in the visible region [116].

6.4. Effect of Annealing Treatment on the PANI–SWCNT Composite

Vibrational and optical behaviors of the hybrid material after annealing were analyzed in a previous study [132]. Interpretation of changes in FTIR spectra has shown the grafting and self-cross-linking of PANI moieties [133,134]. More details of the molecular structure are evidenced by the splitting of the band at 1126 cm^{-1} after annealing (Figure 17(1)). These chemical environments could not be the consequence of CNT insertion (the same line shape appears with and without CNTs). These additional bands are typically coherent with self-cross-linking (Figure 17(2)), such as benzene ring para- and ortho-link, to nitrogen atoms [132].
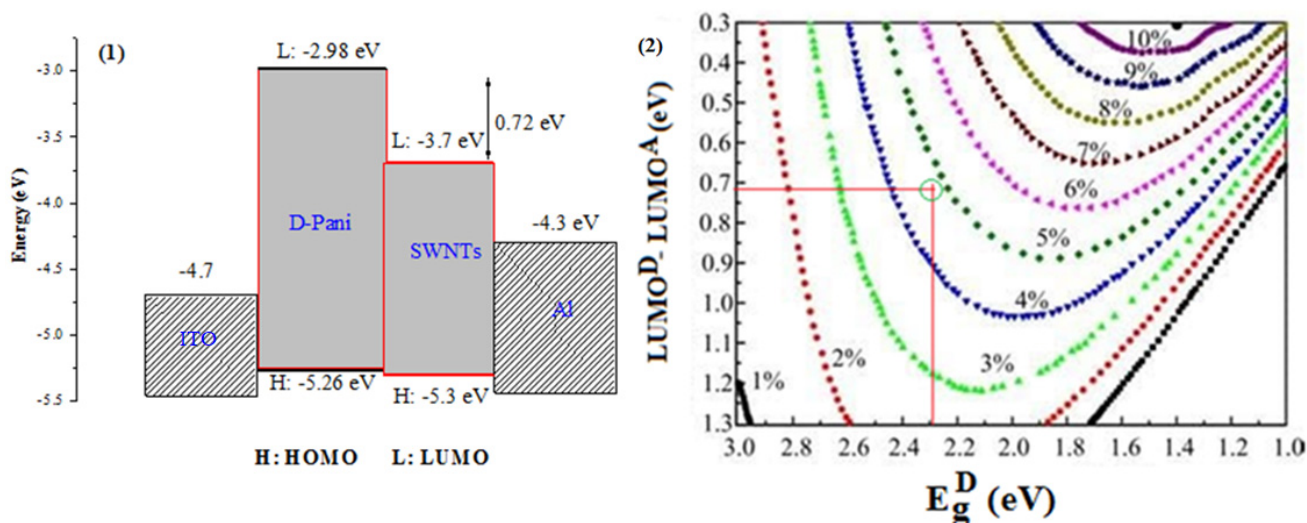
Figure 16. (**1**) Electrode choice for the photovoltaic device. (**2**) Estimation of PCE from the Scharber diagram [19].
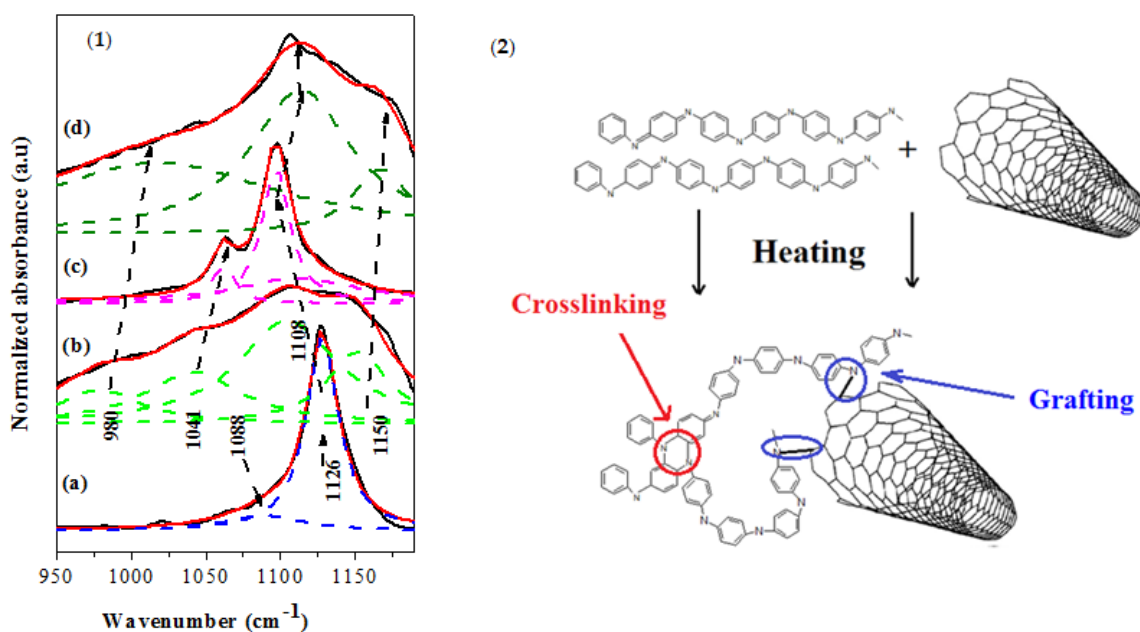
Figure 17. (**1**) Splitting of the FTIR band at 1126 cm^{-1} under annealing: pure PANI (**a**), annealed PANI (**b**), not-annealed composite (**c**), and annealed composite (**d**). (**2**) Structure of the nanocomposite obtained after annealing at 393 K.

After annealing at 393 K, new absorption bands are created at λ_{max} = 570 nm and at λ_{max} = 792 nm, respectively, for doped and functionalized states [132]. These new optical features support the presence of a quinoidal ring and agree well with the self-cross-linking process [135,136]. The direct and indirect band gaps are evaluated from absorbance coefficient data using the Tauc method [137,138]. The direct and indirect energy gaps (Eg) are calculated from the linear dependence of the plot of $(\alpha h\nu)^{1/n}$ versus energy (Figure 18) [139–141].
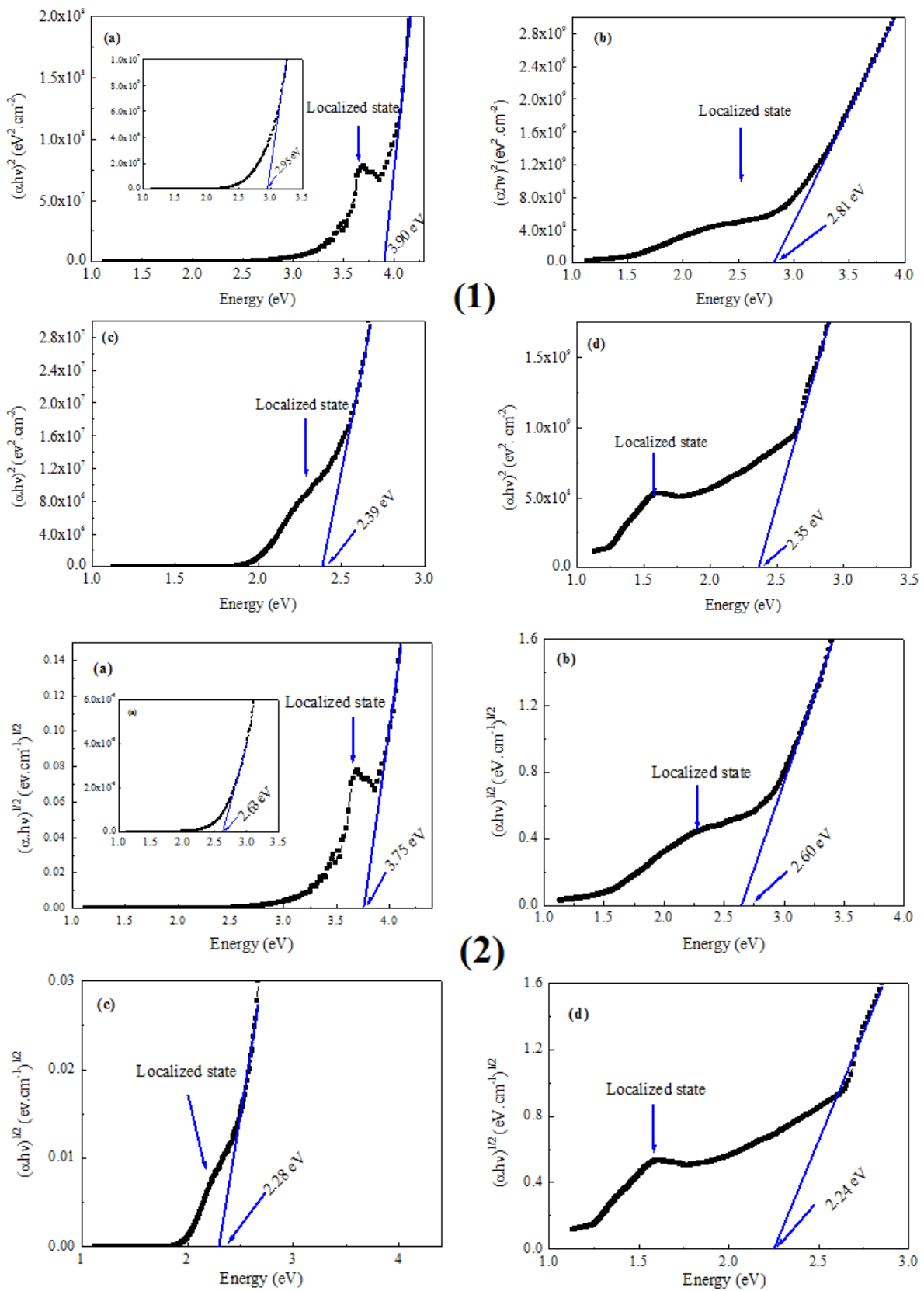
Figure 18. Evaluation of direct (**1**) and indirect (**2**) band gap for doped PANI in the not-annealed (**a**) and annealed (**b**) states and those of the doped PANI/SWCNT composite in the not-annealed (**c**) and annealed (**d**) states. The inset of (**a**) shows the threshold energy of localized states created by doping.

As previously reported, both direct and indirect transition processes dominate optical transitions since direct and indirect energy gaps are nearly similar and the variation $(\Delta E = (E_{Dir} - E_{Ind})/E_{Ind})$ is in the range from 4% to 8% [138]. The value of the transition probability index *n* has been also calculated to evaluate the weight of optical transition mode (values vary from 0.82 to 1.24).

The skin depth variation as a function of incident photon energy is one of the most relevant parameters reflecting the importance of adding CNTs (Figure 19).
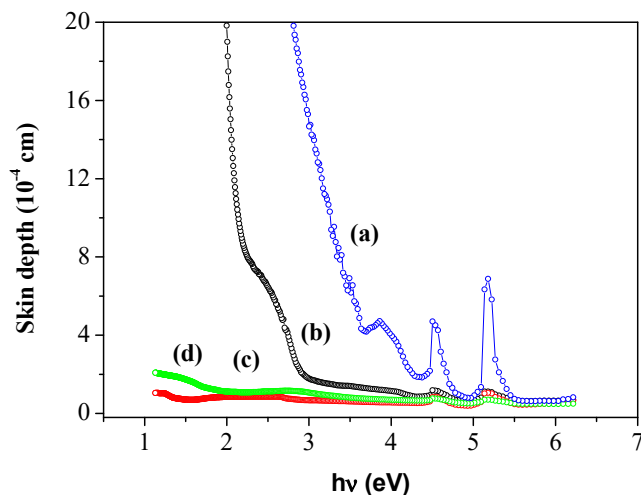
Figure 19. Skin depths of doped PANI: not annealed (**a**) and annealed (**b**); skin depths of doped PANI functionalized with CNTs: not annealed (**c**) and annealed (**d**).

When SWCNTs are added, the skin depth decreases; it decreases further after annealing, indicating the reduction in the transparency volume. This result demonstrates that the addition of CNTs leads to a better interfacial strength, as proved in a previous thermal study [142]. At a higher photon energy, the two picks of skin depth are the signature of plasma frequency, resulting from overlapping between the frequency of electron oscillation and the incident electromagnetic radiation (the wave is stagnant).

The variation in the extinction coefficient versus energy is another indicator of the change in optical properties after the addition of CNTs in both annealed and not-annealed states (Figure 20).
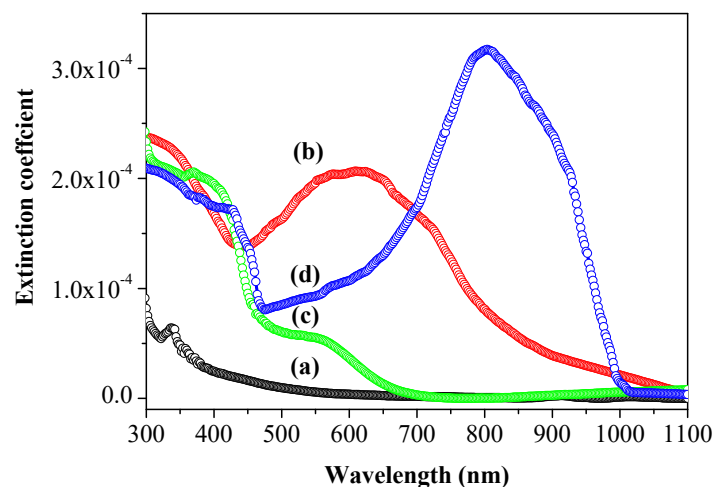
Figure 20. Extinction coefficients of doped PANI: not annealed (**a**) and annealed (**b**). Extinction coefficients of doped PANI functionalized with CNTs: not annealed (**c**) and annealed (**d**).

On the red side of the spectra, annealing improves the extinction coefficient. For the doped state of PANI, thermal treatment leads to a change in the oxidation degree and localized states can overlap with the LUMO level. The extinction coefficient may be improved as a consequence of the new energetic configuration. For the nanocomposite, a net amelioration in the spectral range from 600 to 850 nm is observed after annealing. Indeed, good SWCNT dispersion leads to a covalent bonding, as previously reported [46]. If the overlapping between diffusion length and nanoparticles repartition is satisfied, charge transfer from the doped matrix to CNTs can be established. From Tauc formalism, the calculation of band width of the corresponding localized states (E_U) demonstrates the decrease in the latter when annealing, probably due to the already discussed self-cross-linking effects [133,134,143]. Figure 21 represents all changes in the electronic structure after annealing and adding CNTs.
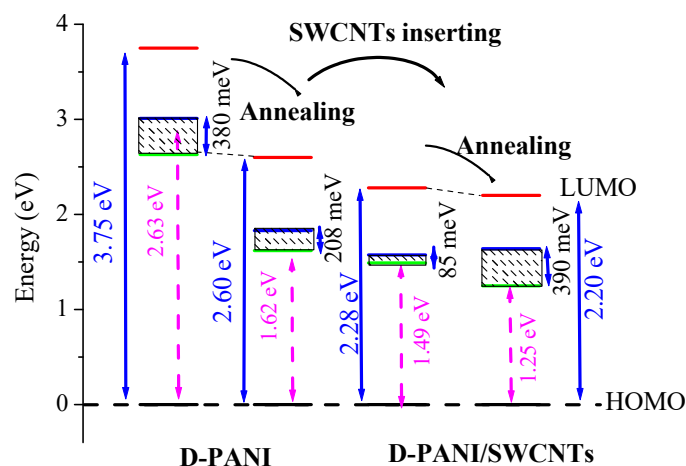
Figure 21. Change in optical parameters under doping and annealing.

For the nanocomposite, the E_U (localized state band width) is nearly 85 meV and 390 eV for not-annealed and annealed states, respectively, involving a charge transfer from the organic matrix (self-cross-linked) to CNTs, as previously reported [21]. The large value after annealing is the consequence of well-dispersed nanoparticles, involving good compatibility between the diffusion length and CNT repartition. A microscopic study mentions that bundled CNTs before annealing became relatively dispersed and homogeneously distributed, with the repartition size varying from 3 to 8 nm [132]. At the molecular scale, annealing leads to partially dispersed and oriented SWCNTs in cross-linked PANI. Electron–hole pairs, which constitute the exciton pairs, are born in the PANI matrix and then migrate by diffusion [20,144]. From the Scharber diagram, the resulting electronic structure presents a band gap suitable for a relatively higher conversion efficiency and is qualified by good compatibility with the solar spectrum [145].

7. Conclusions

A study of the structural, optical, and electronic properties of diverse polymers containing nitrogen atoms was performed. Some parameters are fundamental to achieving better dispersion of CNTs in the organic matrix, namely the choice of the solvent and thermal treatment. Short oligo-N-vinylcarbazole can be spontaneously functionalized with SWCNTs when chloroform is the medium. However, moderate thermal treatment is needed when chlorobenzene is the medium. Though the complete isolation of SWNTs can be achieved, chlorobenzene is more efficient in the SWCNT dispersion process. Correlation of experimental and theoretical study (DFT) in both cases demonstrates that there is a grafting of vinylidene groups to the nanotube side wall. For PVK-P3HT, a good dispersion state is obtained even at a higher SWCNT concentration, reaching 60% of CNTs, and the grafting is limited to the hexylthiophene sequences. The conservation of the hexylthiophene molecular

structure leads to excellent properties for photovoltaic conversion, such as compatibility with the solar spectrum and the effectiveness of the dynamics of the excited states.

PANI itself is an insulating material, because of which its functionalization with CNTs was preceded by acid doping. Without thermal treatment, PANI is linked to SWCNTs via nitrogen atoms, leading to some structural and optical changes. A decrease in the optical gap of 2.28 eV gives rise to good compatibility with the solar spectrum. Moreover, donor–acceptor charge transfer creates a localized state within the band gap, with an onset energy of 1.62 eV. The modeling of a prototype bulk hetero-nanojunction photovoltaic device gives a typical open-circuit voltage of 1.25 V and a PCE of 4~5%. Annealing induces the self-cross-linking of PANI in its doped state and the dispersion of CNTs in the organic matrix. Otherwise, thermal treatment influences the electronic structure, leading to a band gap of 2.20 eV and localized states having a bandwidth of 390 meV. Moreover, it was found that skin depth and extinction coefficient variations are closely related to a molecular arrangement induced by annealing, namely self-cross-linking. As a consequence of the number of oxidation degrees of PANI, the corresponding interpenetrating network (doped PANI/CNTs) exhibits excellent compatibility with the solar spectrum and shows good coherence with the diffusion length, making it a good candidate for the active layer in organic photovoltaic devices.

As a consequence of the above-mentioned structural changes, adding CNTs to the polymer matrix leads to a broader absorption spectrum, PL quenching, and a shorter excited lifetime. In fact, these optical criteria are coherent with charge transfer from the organic matrix to the CNTs due to the interpenetrating P–N nanojunctions.

Author Contributions: Conceptualization, B.Z.; methodology, B.Z., N.S. and M.G.A.; software, B.Z.; formal analysis, B.Z.; investigation B.Z.; resources, B.Z., A.G.A. and S.D.A.; data curation, B.Z.; writing—original draft preparation, B.Z.; writing—review and editing, B.Z., N.S. and A.G.A.; visualization, N.S.; supervision, B.Z.; project administration, B.Z.; funding acquisition, B.Z., M.G.A. and N.S. All authors have read and agreed to the published version of the manuscript.

Institutional Review Board Statement: Not applicable.

Informed Consent Statement: Not applicable.

Data Availability Statement: The data supporting the reported results of this study will be made available by the authors upon request.

Conflicts of Interest: The authors declare no conflict of interest.

References

1. Burroughes, J.H.; Bradley, D.D.C.; Brown, A.R.; Maorks, R.N.; Mackey, K.; Friend, R.H.; Burn, P.L.; Holmes, A.B. Electroluminescence on conjugated polymer. *Nature* **1990**, *397*, 547–569.
2. Saxena, V.; Malhotra, B.D. Prospects of conducting polymers in molecular electronics. *Curr. Appl. Phys.* **2003**, *3*, 293–305. [CrossRef]
3. Han, Y.-K.; Chang, M.-Y.; Ho, K.-S.; Hsieh, T.-H.; Tsai, J.-L.; Huang, P.-C. Electrochemically deposited nano polyaniline films as hole transporting layers in organic solar cells. *Solar Energy Mater. Sol. Cells* **2014**, *128*, 198–203. [CrossRef]
4. Namsheer, K.; Rout, C.S. Conducting polymers: A comprehensive review on recent advances in synthesis, properties and applications. *RSC Adv.* **2021**, *11*, 5659–5697. [CrossRef]
5. Ahllskog, M.; Menon, R.; Heeger, A.J.; Noguchi, T.; Ohnishi, T. Metal-insulator transition in oriented poly(p-phenylenevinylene). *Phys. Rev. B* **1997**, *55*, 6777–6787. [CrossRef]
6. Wang, G.; Morrin, A.; Li, M.; Liu, N.; Luo, X. Nanomaterial-doped conducting polymers for electrochemical sensors and biosensors. *J. Mater. Chem. B* **2018**, *6*, 4173–4190. [CrossRef]
7. Heeger, A.J. Nobel Prize 2000 lecture: Semiconducting and metallic polymers: The fourth generation of polymeric materials. *Curr. Appl. Phys.* **2001**, *1*, 247–267. [CrossRef]

8. Wu, W.; Li, F.; Nie, C.; Wu, J.; Chen, W.; Wu, C.; Guo, T. Improved performance of flexible white hybrid light emitting diodes by adjusting quantum dots distribution in polymer matrix. *Vacuum* **2015**, *111*, 1–4. [CrossRef]

9. Yuanhang, Y.; Hong, Z. Water-induced polymer swelling and its application in soft electronics. *Appl. Surf. Sci.* **2022**, *577*, 151895. [CrossRef]

10. Razykov, T.M.; Ferekides, C.S.; Morel, D.; Stefanakos, E.; Ullal, H.S.; Upadhyaya, H.M. Solar photovoltaic electricity: Current status and future prospects. *Solar Energy* **2011**, *85*, 1580–1608. [CrossRef]

11. Lizin, S.; Passel, S.V.; Schepper, E.D.; Vranken, L. The future of organic photovoltaic solar cells as a direct power source for consumer electronics. *Sol. Energy Mater. Sol. Cells* **2012**, *103*, 1–10. [CrossRef]

12. Deng, P.; Lei, Y.; Zheng, X.; Li, S.; Wu, J.; Zhu, F.; Ong, B.S.; Zhang, Q. Polymer based on benzothiadiazole-bridged bis-isoindigo for organic field-effect transistor applications. *Dyes Pigm.* **2016**, *125*, 407–413. [CrossRef]

13. Tehrani, Z.; Korochkina, T.; Govindarajan, S.; Thomas, D.J.; Mahony, J.O.; Kettle, J.; Claypole, T.C.; Gethin, D.T. Ultra-thin flexible screen printed rechargeable polymer battery for wearable electronic applications. *Org. Electron.* **2015**, *26*, 386–394. [CrossRef]

14. Moaseri, E.; Karimi, M.; Baniadam, M.; Maghreb, M. Improvements in mechanical properties of multi-walled carbon nanotube-reinforced epoxy composites through novel magnetic-assisted method for alignment of carbon nanotubes. *Compos. A Appl. Sci. Manuf.* **2014**, *64*, 228–233. [CrossRef]

15. Mulligan, C.J.; Bilen, C.; Zhou, X.; Belcher, W.J.; Dastoor, P.C. Levelised cost of electricity for organic photovoltaics. *Sol. Energy Mater. Sol. Cells* **2015**, *133*, 26–31. [CrossRef]

16. Subramanyam, B.V.R.S.; Mahakul, P.C.; Sa, K.; Alam, I.; Das, S.; Subudhi, S.; Mandal, M.; Patr, S.; Mahanandi, P. Applications of carbon nanotubes in different layers of P3HT: PCBM bulk heterojunction organic photovoltaic cells. *Mater. Today Proc.* **2021**, *39*, 1862–1865. [CrossRef]

17. Francis, X.P.A.; Benoy, M.D.; Stephen, S.K.; Varghese, T. Enhanced electrical properties of polyaniline carbon nanotube composites: Analysis of temperature dependence of electrical conductivity using variable range hopping and fluctuation induced tunneling models. *J. Solid State Chem.* **2021**, *300*, 122232. [CrossRef]

18. Zaidi, B.; Bouzayen, N.; Znaidia, S.; Mbarek, M.; Massuyeau, F.; Faulques, E.; Gautron, E.; Wery, J.; Duvail, J.L.; Ghedira, M.; et al. Dynamic properties of the excited states of oligo-N-vinylcarbazole functionalized with single walled carbon nanotubes. *J. Mol. Struct.* **2013**, *1039*, 46–50. [CrossRef]

19. Saoudi, M.; Ajjel, R.; Zaidi, B. Experimental and theoretical study on the charge transfer between polyaniline and single walled carbon nanotube. *J. Mater. Environ. Sci.* **2016**, *7*, 4435–4447.

20. Saaidia, A.; Saidani, M.A.; Romdhane, S.; BenFredj, A.; Egbec, D.A.M.; Tekin, E.; Bouchriha, H. Morphology-dependent exciton diffusion length in PPE-PPVs thin films as revealed by a Forster mechanism based-study. *Synth. Met.* **2017**, *226*, 177–182. [CrossRef]

21. Zaidi, B.; Bouzayen, N.; Wéry, J.; Alimi, K. Grafting of oligo-N-vinyl carbazole on single walled carbon nanotubes. *J. Mol. Str.* **2010**, *97*, 71–80. [CrossRef]

22. Ferguson, A.J.; Blackburn, J.L.; Kopidakis, N. Fullerene and carbon nanotubes as acceptor materials in organic photovoltaic. *Mater. Lett.* **2013**, *90*, 115–125. [CrossRef]

23. Gao, G.; Yu, J.; Hummelen, J.C.; Wudl, F.; Heeger, A.J. Polymer Photovoltaic Cells: Enhanced Efficiencies via a Network of Internal Donor-Acceptor Heterojunctions. *Science* **1995**, *270*, 1789–1791. [CrossRef]

24. Janssen, R.A.J.; Hummelen, J.C.; Sariciftci, N.S. Polymer–Fullerene Bulk Heterojunction Solar Cells. *MRS Bull.* **2005**, *30*, 33–36. [CrossRef]

25. Sun, Y.; Zhang, W.; Chi, H.J.; Liu, Y.; Hou, C.L.; Fang, D. Recent development of graphene materials applied in polymer solar cell, Renew. *Sust. Energ. Rev.* **2015**, *43*, 973–980. [CrossRef]

26. Neeraj, K.; Pushpendra, S. Review of next generation photovoltaic solar cell technology and comparative materialistic development. *Mater. Today Proc.* **2021**; *in press*. [CrossRef]

27. Anindya, S.; Nibedita, S.; Gautam, M. Fabrication and Characterization of Flexible Semi-conducting Nanocomposite Polymer. *Ref. Modul. Mater. Sci. Mater. Eng.* **2022**; *in press*. [CrossRef]

28. Huang, Y.Y.; Terentjev, E.M. Dispersion of Carbon Nanotubes: Mixing, Sonication Stabilization, and Composite Properties, Polymers. *Polymers* **2012**, *4*, 275–295. [CrossRef]

29. Alimi, K.; Zaidi, B.; Chemek, M. About Grafting of Single-walled Carbon Nanotubes on the Oligo-N-vinyl Carbazole and Copolymer Involving N-vinylcarbazole and Hexylthiophene. In *Carbon Nanotubes—Polymer Nanocomposites*; Intech: London, UK, 2011; pp. 300–330. [CrossRef]

30. Sandler, J.; Shaffer, M.S.P.; Prasse, T.; Bauhfer, W.; Schulte, K.; Windle, H. Development of a dispersion Process for carbon nanotubes in an epoxy matrix and the resulting electrical properties. *Polymer* **1999**, *40*, 5967–5971. [CrossRef]

31. Park, S.D.; Han, D.H.; Teng, D.; Kwon, Y. Rheological properties and dispersion of multi-walled Carbon nanotube (MWCNT) in polystyrene matrix. *Curr. Appl. Phys.* **2008**, *8*, 482–485. [CrossRef]

32. Chen, G.X.; Li, Y.; Shimizu, H. Ultrahigh-shear processing for the preparation of polymer/carbon nanotube composites. *Carbon* **2007**, *45*, 2334–2340. [CrossRef]

33. Moradi, O.; Yari, M.; Zare, K.; Mizra, B.; Najafi, F. A review of chemistry principles and reactions. *Fuller. Nanotub. Carbon Nanostructures* **2012**, *20*, 138–151. [CrossRef]

34. Liu, J.Q.; Xiao, T.; Liao, K.; Wu, P. Interfacial design of carbon nanotube polymer composites: A hybrid system of noncovalent and covalent functionalizations. *Nanotechnology* **2012**, *18*, 165701. [CrossRef]

35. Viswanathan, G.; Chakrapani, N.; Yang, H.; Wei, B.; Chung, H.; Cho, K.; Chang, Y.R.; Ajayan, P.M. Single-step in situ synthesis of polymer-grafted single-wall nanotube composites. *J. Am. Chem. Soc.* **2003**, *125*, 9258–9259. [CrossRef] [PubMed]

36. Holzinger, M.; Steinmetz, J.; Samaille, D.; Glerup, M.; Paillet, M.; Bernier, P.; Ley, L.; Graupner, R. Cycloaddition for cross-linking SWCNTs. *Carbon* **2004**, *42*, 941–947. [CrossRef]

37. Peng, H.; Reverdy, P.; Khabashesku, V.N.; Margrave, J.L. Side wall functionalization of single- walled carbon nanotubes with organic peroxides. *Chem. Commun.* **2003**, *3*, 362–365. [CrossRef]

38. Martin, R.; Céspedes-Guirao, F.J.; Miguel, M.D.; Lazaro, F.F.; García, H.; Sastre, S.A. Single- and multi-walled carbon nanotubes covalently linked to Synthesis, characterization and photophysical properties. *Chem. Sci.* **2012**, *3*, 470–475. [CrossRef]

39. Andreas, H. Functionalization of Single-Walled Carbon Nanotubes. *Chem. Int. Ed.* **2012**, *41*, 1853–1859. [CrossRef]

40. Shanmugharaj, A.M.; Bae, J.H.; Nayak, R.R.; Ryu, S.H. Preparation of poly(styrene-co-acrylonitrile)-grafted multiwalled carbon nanotubes via surface-initiated atom transfer radical polymerization. *J. Polym. Sci. A Polym. Chem.* **2007**, *45*, 460–470. [CrossRef]

41. Qin, S.; Qin, D.; Ford, W.T.; Resasco, D.E.; Herrera, J.E. Functionalization of single-walled carbon nanotubes with polystyrene via grafting to and grafting from method. *Macromolecules* **2004**, *37*, 752–757. [CrossRef]

42. Vijayakumar, C.; Balan, B.; Kim, M.J.; Takeuchi, M. Noncovalent Functionalization of SWNTs with Azobenzene-Containing Polymers: Solubility, Stability, and Enhancement of Photoresponsive Properties. *ACS J. Phys. Chem. C* **2011**, *115*, 4533–4539. [CrossRef]

43. Rajarajeswari, M.; Iyakutti, K.; Kawazoe, Y. Noncovalent and radicals covalent functionalization of a (5, 0) single-walled carbon nanotube with alanine and alanine. *J. Mol. Model.* **2012**, *18*, 771–781. [CrossRef] [PubMed]

44. Kong, J.; Yenilmez, E.; Tombler, T.W.; Kim, W.; Dai, H. Quantum interference and ballistic transmission in nanotube electron waveguides. *Phys. Rev. Lett.* **2001**, *87*, 106801–106807. [CrossRef] [PubMed]

45. Deng, J.; Ding, X.; Zhang, W.; Peng, Y.; Wang, J.; Long, X.; Li, P.; Chan, A. Carbon nanotube–polyaniline hybrid materials. *Eur. Polym. J.* **2002**, *38*, 2497–2501. [CrossRef]

46. Sahoo, N.G.; Jung, Y.C.; So, H.H.; Chob, J.W. Polypyrrole Coated Carbon Nanotubes: Synthesis, Characterization, and Enhanced Electrical Properties. *Synth. Met.* **2007**, *157*, 374–379. [CrossRef]

47. Kerr, C.J.; Huang, Y.Y.; Marshall, J.E.; Terentjev, E.M. Effect of filament aspect ratio on the dielectric response of multiwalled carbon nanotube composites. *J. Appl. Phys.* **2011**, *109*, 094109. [CrossRef]

48. Pietro, W.J.; Francl, M.M.; Hehre, W.J.; Defrees, D.J.; Pople, J.A.; Binkley, J.S. Self-consistent molecular orbital methods. 24. Supplemented small split-valence basis sets for second-row elements. *J. Am. Chem. Soc.* **1982**, *104*, 5039–5048. [CrossRef]

49. Pickholz, M.; dos Santos, M.C. Interchain and correlation effects in oligothiophenes. *Synh. Met.* **1999**, *101*, 528–529. [CrossRef]

50. DiCesare, N.; Belletete, M.; Marrano, C.; Leclerc, M.; Durocher, G. Conformational Analysis (ab initio HF/3-21G*) and Optical Properties of Symmetrically Disubstituted Terthiophenes. *J. Phys. Chem. A* **1998**, *102*, 5142–5149. [CrossRef]

51. Ayachi, S.; Alimi, K.; Bouachrine, M.; Hamidi, M.; Mevellec, J.Y.; Porte, J.P.L. Spectroscopic investigations of copolymers incorporating various thiophene and phenylene monomers. *Synth. Met.* **2006**, *156*, 318–326. [CrossRef]

52. Zou, L.Y.; Ren, A.M.; Feng., J.K.; Ran, X.Q.; Liu, Y.L.; Sun, C.C. Structural, electronic, and optical properties of phenol-pyridyl boron complexes for light-emitting diodes. *Int. J. Quantum Chem.* **2009**, *109*, 1419–1429. [CrossRef]

53. Khoshkholgh, M.J.; Marsusi, F.; Abolhassani, M.R. Density functional theory investigation of opto-electronic properties of thieno [3,4-b] thiophene and benzodithiophenepolymer and derivatives and their applications in solar cell. *Spectrochim. Acta Part A* **2015**, *136*, 373–380. [CrossRef] [PubMed]

54. Zhengkun, D.; Mian, C.; Li, D.; Baojin, H.; Zhong, C.; Donghong, Y.; Meng, C.L. Effect of alkylthiolated hetero-aromatic rings on the photovoltaic performance of benzodithiophene-based polymer/fullerene solar cells. *Synt. Met.* **2021**, *276*, 116756. [CrossRef]

55. Zhang, L.; Wan, M. Self-Assembly of Polyaniline—From Nanotubes to Hollow Microspheres. *Adv. Funct. Mater.* **2003**, *13*, 815–820. [CrossRef]

56. Bonard, J.M.; Stora, T.; Salvetat, J.P.; Maier, F.; Stockli, T.; Dusch, C.; Forró, L.; Châtelain, A. Purification and size selection of carbon nanotubes. *Adv. Mater.* **1997**, *9*, 827–831. [CrossRef]

57. Hu, H.; Yu, A.; Kim, E.; Zhao, B.; Itkis, M.E.; Bekyarova, E.; Haddon, R.C. Influence of the Zeta Potential on the Dispersability and Purification of Single-Walled Carbon Nanotubes. *J. Phys. Chem. B* **2005**, *109*, 11520–11524. [CrossRef] [PubMed]

58. Wang, Y.; Gao, L.; Sun, J.; Liu, Y.; Zheng, S.; Kajiura, H. An integrated route for purification, cutting and dispersion of single-walled carbon nanotubes. *Chem. Phys. Lett.* **2006**, *432*, 205–208. [CrossRef]

59. Arnold, M.S.; Green, A.A.; Hulvat, J.F.; Stupp, S.I.; Hersam, M.C. Sorting carbon nanotubes by electronic structure using density differentiation. *Nat. Nanotechnol.* **2006**, *1*, 60–65. [CrossRef]

60. Arnold, M.S.; Stupp, S.I.; Hersam, M.C. Enrichment of single-walled carbon nanotubes by diameter. *Nano Lett.* **2005**, *5*, 713–718. [CrossRef]

61. Strano, M.S.; Dyke, C.A.; Usrey, M.L.; Barone, P.W.; Allen, M.J.; Shan, H.; Kittrell, C.; Hauge, R.H.; Tour, J.M.; Smalley, R.E. Electronic Structure Control of Single-Walled Carbon Nanotube Functionalization. *Science* **2003**, *301*, 1519–1522. [CrossRef]

62. Kyoichi, O.; Masahiko, M.; Yoshihiro, T. Analysis of the dispersion state of pitch particles in polymers for nanofiber fabrication by optical microscopy and image processing. *J. Phys. Chem. Solids* **2022**, *163*, 110585. [CrossRef]

63. Becke, A.D.J. Density-functional thermochemistry. III. The role of exact exchange. *Chem. Phys.* **1993**, *98*, 5648. [CrossRef]

64. Futaba, D.N.; Mizuno, K.; Namai, T.; Yumura, M.; Iijima, S. Water-assisted highly efficient synthesis of impurity-free single-walled carbon nanotubes. *Science* **2004**, *306*, 1362–1364. [CrossRef]

65. Meyyappan, M.; Delzeit, L.; Cassell, A.; Hash, D. Carbon nanotube growth by PECVD: A review. *Plasma Sources Sci. Technol.* **2003**, *12*, 205. [CrossRef]

66. Zhang, Y.; Iijima, S. Elastic reponse of carbon nanotube bundles to visible light. *Phys. Rev. Lett.* **1999**, *82*, 3472. [CrossRef]

67. Rarvikar, N.R.; Schadler, L.S.; Vijaaraghavan, A.; Zhao, Y.; Wei, B.; Ajayan, P.M. Synthesis and characterization of thickness-aligned carbon nanotube-polymer composite films. *Chem. Mater.* **2005**, *17*, 974–983. [CrossRef]

68. Boncel, S.; Koziol, K.K.K.; Walczak, K.Z.; Windle, A.H.; Shaffer, M.S.P. Infiltration of highly aligned carbon nanotube arrays with molten polystyrene. *Mater. Lett.* **2011**, *65*, 2229–2303. [CrossRef]

69. Chen, Y.; Yu, J. Growth direction control of aligned carbon nanotubes. *Carbon* **2005**, *43*, 3181–3194. [CrossRef]

70. Chen, X.Q.; Saito, T.; Yamada, H.; Matsushige, K. Aligning singlewall carbon nanotubes with an alternating- current electric field. *Appl. Phys. Lett.* **2001**, *78*, 3714–3716. [CrossRef]

71. Domingues, D.; Logakis, E.; Skordos, A.A. The use of an electric field in the preparation of glass fibre/epoxy composites containing carbon nanotubes. *Carbon* **2012**, *50*, 2493–2503. [CrossRef]

72. Hone, J.; Llaguno, M.C.; Nemes, N.M.; Johnson, A.T.; Fischer, J.E.; Walters, D.A. Electrical and thermal transport properties of magnetically aligned single wall carbon nanotube films. *Appl. Phys. Lett.* **2000**, *77*, 666–668. [CrossRef]

73. Choi, E.S.; Brooks, J.S.; Eaton, D.L.; Al-Haik, M.S.; Hussaini, M.Y.; Garmestani, H.; Li, D.; Dahmen, K. Enhancement of thermal and electrical properties of carbon nanotube polymer composites by magnetic field processing. *J. Appl. Physiol.* **2003**, *94*, 6034–6039. [CrossRef]

74. Dimaki, M.; Bøggild, P. Dielectrophoresis of carbon nanotubes using microelectrodes: A numerical study. *Nanotechnology* **2004**, *15*, 1095–1102. [CrossRef]

75. Zhan, H.; Chen, Y.W.; Shi, Q.Q.; Zhang, Y.; Mo, R.W.; Wang, J.N. Highly aligned and densified carbon nanotube films with superior thermal conductivity and mechanical strength. *Carbon* **2022**, *186*, 205–214. [CrossRef]

76. Monti, M.; Natali, M.; Torre, L.; Kenny, J.M. The alignment of single walled carbon nanotubes in an epoxy resin by applying a DC electric field. *Carbon* **2012**, *50*, 2453–2464. [CrossRef]

77. Zhokhavets, U.; Erb, T.; Hoppe, H.; Gobsch, G.; Sariciftci, N.S. Effect of annealing of poly(3-hexylthiophene)/fullerene bulk heterojunction composites on structural and optical properties. *Thin Solid Film* **2006**, *496*, 679–682. [CrossRef]

78. Yang, X.; Loos, J.; Veenstra, S.C.; Verhees, W.J.H.; Wienk, M.M.; Kroon, J.M.; Michels, M.A.J.; Janssen, R.A.J. Nanoscale Morphology of High-Performance Polymer Solar Cells. *Nano Lett.* **2005**, *5*, 579–583. [CrossRef]

79. Savenije, T.J.; Kroeze, J.E.; Yang, X.; Loos, J. The formation of crystalline P3HT fibrils upon annealing of a PCBM:P3HT bulk heterojunction. *Thin Solid Film.* **2006**, *511–512*, 2–6. [CrossRef]

80. Zhu, H.; Wei, J.; Wang, K.; Wu, D. Applications of carbon materials in photovoltaic solar cells. *Sol. Energy Mater. Sol. Cells* **2009**, *93*, 1461–1470. [CrossRef]

81. Yun, D.; Feng, W.; Wu, H.; Li, B.; Liu, X.; Yi, W.; Qiang, J.; Gao, S.; Yan, S. Controllable functionalization of single-wall carbon nanotubes by in situ polymerization method for organic photovoltaic device. *Synt. Met.* **2008**, *158*, 977–983. [CrossRef]

82. Derbal-Habak, H.; Bergeret, C.; Cousseau, J.; Nunz, J.M. Improving the current density Jsc of organic solar cells P3HT:PCBM by structuring the photoactive layer with functionalized SWCNTs. *Sol. Energy Mater. Sola. Cells* **2011**, *95*, 553–556. [CrossRef]

83. Jun, G.H.; Jin, S.H.; Park, S.H.; Jeon, S.; Hong, S.H. Highly dispersed carbon nanotubes in organic media for polymer: Fullerene photovoltaic devices. *Carbon* **2012**, *50*, 40–46. [CrossRef]

84. Rajiv, K.; Jitendra, K.; Amit, K.; Vikram, K.; Rama, K.; Ramadhar, S. Poly(3-hexylthiophene):Functionalized single-walled carbon nanotubes: (6,6)-phenyl-C61-butyric acidmethyl ester composites for photovoltaic cell at ambient condition. *Sol. Energy Mater. Sol. Cells* **2010**, *94*, 2386–2394. [CrossRef]

85. Shaheen, S.E.; Brabec, C.J.; Sariciftci, N.S.; Padinger, F.; Fromherzet, T.; Hummelen, J.C. 2.5% efficient organic plastic solar cells. *Appl. Phys. Lett.* **2001**, *78*, 841–843. [CrossRef]

86. Peumans, P.; Forrest, S.R. Very-high-efficiency double-heterostructure copper phthalocyanine/C60 photovoltaic cells. *Appl. Phys. Lett.* **2001**, *79*, 126–128. [CrossRef]

87. Xue, M.A.; Uchida, S.; Rand, B.P.; Forrest, S.R. 4.2% efficient organic photovoltaic cells with low series resistances. *Appl. Phys. Lett.* **2004**, *84*, 3013–3015. [CrossRef]

88. Cui, Y.; Yao, H.; Hong, L.; Zhang, T.; Tang, Y.; Lin, B.; Xian, K.; Gao, B.; An, C.; Bi, P.; et al. 17% efficiency organic photovoltaic cell with superior processability. *Nat. Sci. Rev.* **2020**, *7*, 1239–1246. [CrossRef]

89. Wu, W.; Li, J.; Liu, L.; Yanga, L.; Guo, Z.-X.; Dai, L.; Zhu, D. The photoconductivity of PVK-carbon nanotube blends. *Chem. Phys. Lett.* **2002**, *364*, 196–199. [CrossRef]

90. Bernede, J.C.; Alimi, K.; Safoula, G. Influence of annealing treatment on iodine doped poly(N-vinylcarbazole) powders. *Polym. Deg. Stab.* **1994**, *46*, 269–274. [CrossRef]

91. Napo, K.; Chand, S.; Bernede, J.C.; Safoula, G.; Alimi, K. Growth and characterization of vacuum-deposited polyvinylcarbazole (PVK) films. *J. Mat. Sci.* **1992**, *27*, 6219–6222. [CrossRef]

92. Touihri, S.; Safoula, G.; Leny, R.; Bernede, J.C. Comparison of the properties of iodine-doped poly(N-vinylcarbazole)(PVK) thin films obtained by evaporation of pure powder followed by iodine post-deposition doping and iodine pre-doped powder. *Thin Solid Film.* **1997**, *304*, 16–23. [CrossRef]

93. Lee, C.; Yang, W.; Parr, R.G. Development of the Colle-Salvetti correlation-energy formula into a functional of the electron density. *Phys. Rev. B* **1988**, *37*, 785–789. [CrossRef] [PubMed]

94. Massuyeau, F.; Faulques, E.; Lefrant, S.; Majdoub, M.; Ghedira, M.; Alimi, K.; Wéry, J. Photoluminescence properties of new PPV derivatives. *J. Lumin.* **2011**, *131*, 1541–1544. [CrossRef]

95. Mbarek, M.; Zaidi, B.; Alimi, K. Theoretical study of the alkoxyls groups effect on PPV-ether excited states, a relationship with femtosecond decay. *Spectrochim. Acta A Mol. Biomol. Spectrosc.* **2012**, *88*, 23–30. [CrossRef]

96. Zaidi, B.; Bouzayen, N.; Wéry, J.; Alimi, K. Annealing treatment and carbon nanotubes concentration effects on the optical and vibrational properties of single walled carbon nanotubes functionalized with short oligo-N-vinyl carbazole. *Mter. Chem. Phys.* **2011**, *126*, 417–423. [CrossRef]

97. Baibarac, M.; Cantu, M.L.; Sol, J.O.; Baltog, I.; Pastor, N.C.; Romero, P.G. Poly(N-vinyl carbazole) and carbon nanotubes based composites and their application to rechargeable lithium batteries. *Compos. Sci. Technol.* **2007**, *67*, 2556–2563. [CrossRef]

98. Wang, C.; Guo, Z.X.; Fu, S.; Wu, W.; Zhu, D. Polymers containing fullerene or carbon nanotube structures. *Prog. Polym. Sci.* **2004**, *29*, 1079–1141. [CrossRef]

99. Yang, L.; Feng, J.-K.; Ren, A.-M.; Sun, J.-Z. The electronic structure and optical properties of carbazole-based conjugated oligomers and polymers, a theoretical investigation. *Polymers* **2006**, *47*, 1397–1404. [CrossRef]

100. Baibarac, M.; Baltog, I.; Lefrant, S. Raman spectroscopic evidence for interfacial interactions in poly(bithiophene)/single-walled carbon nanotube composites. *Carbon* **2009**, *47*, 1389–1398. [CrossRef]

101. Eklund, P.C.; Holden, J.M.; Jishi, R.A. Vibrational modes of carbon nanotubes; spectroscopy and theory. *Carbon* **1995**, *33*, 959–972. [CrossRef]

102. Huang, J.E.; Li, X.H.; Xu, J.C.; Li, H.L. Well-dispersed single-walled carbon nanotube/polyaniline composite films. *Carbon* **2003**, *41*, 2731–2736. [CrossRef]

103. Lukin, L.V. Efficiency of exciton dissociation at the interface between a conjugated polymer and an electron acceptor with consideration for a two-dimensional arrangement of interfacial dipoles. *Chem. Phys.* **2021**, *551*, 111327. [CrossRef]

104. Baibarac, M.; Baltog, I.; Lefrant, S.; Mevellec, J.Y.; Bucur, C. Vibrational and photoluminescence properties of the polystyrene functionalized single-walled carbon nanotubes. *Diam. Relat. Mater.* **2008**, *17*, 1380–1388. [CrossRef]

105. Ago, H.; Petritsch, K.; Shaffer, M.S.P.; Windle, A.H.; Friend, R.H. Composites of carbon nanotubes and conjugated polymers for photovoltaic devices. *Adv. Mater.* **1999**, *11*, 128–1285. [CrossRef]

106. Mulazzi, E.; Perego, R.; Aarab, H.; Mihut, L.; Lefrant, S.; Faulques, E.; Wéry, J. Photoconductivity and optical properties in composites of poly(paraphenylene vinylene) and single-walled carbon nanotubes. *Phys. Rev. B* **2004**, *70*, 155206–155214. [CrossRef]

107. Lin, Y.-Y.; Chen, C.-W.; Chang, T.Y.; Lin, J.; Liu, I.S.; Su, W.-F. Exciton dissociation and migration in enhanced order conjugates polymer/nanoparticlehybrid materials. *Nanotechnology* **2006**, *17*, 1260–1263. [CrossRef]

108. Lin, Y.-T.; Zeng, T.-W.; Lai, W.-Z.; Chen, C.-W. Efficient photoinduced charge transfer in tio2 nanorod/conjugated polymer hybrid materials. *Nanotechnology* **2006**, *17*, 5781–5785. [CrossRef]

109. Aarab, H.; Baitoul, M.; Wery, J.; Almairac, R.; Lefrant, S.; Faulques, E.; Duvail, J.L.; Hamedoun, M. Electrical and optical properties of PPV and single-walled carbon nanotubes composites films. *Synth. Met.* **2005**, *155*, 63–67. [CrossRef]

110. Ho, Y.B.; In, J.; Chung, H.-K.S.; Chung, Y.K. The effects of alkyls side-chain length and shape of polyfluorenes on the photoluminescence spectra and the fluorescence lifetimes of polyflorene blends with poly(n-vinyl carbazole). *Chem. Phys. Lett.* **2004**, *393*, 197–203. [CrossRef]

111. Massuyeau, F.; Aarab, H.; Mihut, L.; Lefrant, S.; Faulques, E.; Wéry, J. Optical Properties of Poly(para-phenylenevinylene) and single-walled Carbon Nanotube composite films: Effects of conversion temperature, prucursor dilution and nanotube concentrations. *Phys. Chem. C* **2007**, *111*, 15111–15118. [CrossRef]

112. Chemek, M.; Wéry, J.; Bouachrine, M.; Paris, M.; Lefrant, S.; Alimi, K. Synthesis and characterization of novel graft copolymers of Poly(N-vinylcarbazole) and Poly(3-methylthiophene) for optoelectronic applications. *Synth. Met.* **2010**, *160*, 2306–2314. [CrossRef]

113. Craley, C.R.; Zhang, R.; Kowalewski, T.; McCullough, R.D.; Stefan, M.C. Regioregular Poly(3-exylthiophene) in a Novel Conducting Amphiphilic Block Copolymer. *Macromol. Rapid Commun.* **2009**, *30*, 11–16. [CrossRef] [PubMed]

114. McCullough, R. The Chemistry of Conducting Polythiophenes. *Adv. Mater.* **1998**, *10*, 93–116. [CrossRef]

115. Wéry, J.; Aarab, H.; Lefrant, S.; Faulques, E.; Mulazzi, E.; Perego, R. Photoexcitations in compositrs of poly(paraphenylene vinylene) and single—walled carbon nanotubes. *Phys. Rev. B* **2003**, *67*, 115202–115207. [CrossRef]

116. Saoudi, M.; Zaidi, B.; Alotaibi, A.A.; Althobaiti, M.G.; Alosime, E.M.; Ajjel, R. Polyaniline: Doping and Functionalization with Single Walled Carbon Nanotubes for Photovoltaic and Photocatalytic Application. *Polymers* **2021**, *13*, 2595. [CrossRef]

117. Chiang, J.-C.; MacDiarmid, A.G. Polyaniline: Protonic acid doping of the emeraldine form to the metallic regime. *Synth. Met.* **1986**, *13*, 193. [CrossRef]

118. Mishra, A.K.; Tandon, P. A Comparative Ab Initio and DFT Study of Polyaniline Leucoemeraldine Base and Its Oligomers. *J. Phys. Chem. B* **2009**, *113*, 14629. [CrossRef]

119. Baibarac, M.; Baltog, I.; Lefrant, S.; Mevellec, J.Y.; Chauvet, O. Polyaniline and carbon nanotubes based composites containing whole units and fragments of nanotubes. *Chem. Mater.* **2003**, *15*, 4149–4156. [CrossRef]

120. Pal, G.; Kumar, S. Modeling of carbon nanotubes and carbon nanotube–polymer composites. *Prog. Aerosp. Sci.* **2016**, *80*, 33. [CrossRef]

121. Lu, X.; Hu, Y.; Wang, L.; Guo, Q.; Chen, S.; Hou, H.; Song, Y. Macroporous Carbon/Nitrogen-doped Carbon Nanotubes/Polyaniline Nanocomposites and Their Application in Supercapacitors. *Electrochim. Acta.* **2016**, *189*, 158–165. [CrossRef]

122. Byron, P.R.; Hubert, P.; Salvetat, J.-P.; Zalamea, L. Flexural deflection as a measure of van der Waals interaction forces in the CNT array. *Compos. Sci. Technol.* **2006**, *66*, 1125. [CrossRef]

123. Schroder, E.; Hyldgaard, P. The van der Waals interactions of concentric nanotubes. *Mater. Sci. Eng. C* **2003**, *23*, 721. [CrossRef]

124. He, B.; Tang, Q.; Luo, J.; Li, Q.; Chen, X.; Cai, H. Rapid charge-transfer in polypyrrole–single wall carbon nanotube complex counter electrodes: Improved photovoltaic performances of dye-sensitized solar cells. *J. Power Sources* **2014**, *256*, 170–177. [CrossRef]

125. Goswami, M.; Ghosh, R.; Maruyama, T.; Meikap, A.K. Polyaniline/carbon nanotube/CdS quantum dot composites with enhanced optical and electrical properties. *Appl. Surf. Sci.* **2016**, *364*, 176. [CrossRef]

126. El Malki, Z.; Bouachrine, M.; Hamidi, M.; Serein-Spirau, F.; Lere-Porte, J.P.; Sotiropoulos, J.M. Theoretical study of New Donor-π-Acceptor compounds based on Carbazole, Thiophene and Benzothiadiazole for Photovoltaic application as Dyesensitized solar cells. *J. Mater. Environ. Sci.* **2016**, *7*, 324–3255.

127. Aleman, C.; Ferreir, C.A.; Torras, J.; Meneguzzi, A.; Canales, M.; Rodrigues, M.A.S.; Casanovas, J. On the molecular properties of polyaniline: A comprehensive theoretical study. *J. Polym.* **2008**, *49*, 5169. [CrossRef]

128. Gadisa, A.; Svensson, M.; Andersson, M.R.; Inganas, O. Correlation between oxidation potential and open-circuit voltage of composite solar cells based on blends of polythiophenes/fullerene derivative. *Appl. Phys. Lett.* **2004**, *84*, 1609. [CrossRef]

129. Veldman, A.; Meskers, S.C.J.; Janssen, R.A.J. The Energy of Charge-Transfer States in Electron Donor–Acceptor Blends: Insight into the Energy Losses in Organic Solar Cells. *Adv. Funct. Mater.* **2009**, *19*, 1939–1948. [CrossRef]

130. Scharber, M.C.; Sariciftci, N.S. Efficiency of bulk-heterojunction organic solar cells. *Prog. Polym. Sci.* **2013**, *38*, 1929–1940. [CrossRef]

131. Azazi, A.; Mabrouk, A.; Alimi, K. Theoretical investigation on the photophysical properties of low-band-gap copolymers for photovoltaic devices Comput. *Theor. Chem.* **2011**, *978*, 7. [CrossRef]

132. Saoudi, M.; Zaidi, B.; Ajjel, R. Correlation between microstructures and optical properties of polyaniline/single-walled carbon nanotubes composites. *Polym. Compos.* **2019**, *40*, E821–E831. [CrossRef]

133. Rozlivkova, Z.; Trchova, M.; Exnerova, M.; Stejska, J. The carbonization of granular polyaniline to produce nitrogen-containing carbon. *Synt. Met.* **2011**, *161*, 11–22. [CrossRef]

134. Liu, D.; Wang, H.; Du, P.; Liu, P. Independently double-crosslinked carbon nanotubes/polyaniline composite films as flexible and robust free-standing electrodes for high-performance supercapacitors. *Carbon* **2017**, *122*, 761–774. [CrossRef]

135. Borah, R.; Banerjee, S.; Kumar, A. Surface functionalization effects on structural, conformational, and optical properties of polyaniline nanofibers. *Synth. Met.* **2014**, *197*, 225–232. [CrossRef]

136. Verma, D.; Dutt, V. Novel microstructure in spin coated polyaniline thin films. *J. Phys. Condens. Matter.* **2007**, *19*, 186–212. [CrossRef]

137. Tauc, J. *Amorphous and Liquid Semiconductors*; Plenum: New York, NY, USA, 1974.

138. Mathew, A.M.; Predeep, P. Plasma-polymerized elastomer/conducting polymer composite: Structural and optical characterization. *Polym. Compos.* **2013**, *34*, 1091–1098. [CrossRef]

139. Kabir, H.; Rahman, M.M.; Uddin, K.M.; Bhuiya, A.H. Structural, morphological, compositional and optical studies of plasma polymerized 2-furaldehyde amorphous thin films. *Appl. Surf. Sci.* **2017**, *423*, 983–994. [CrossRef]

140. Chithralekha, P.; Subramanian, E.; Padiyan, D.P. Electrodeposition of polyaniline thin films doped with dodeca tungstophosphoric acid: Effect on annealing and vapor sensing. *Sens. Actuators B Chem.* **2007**, *122*, 274. [CrossRef]

141. Banerjee, S.; Kumar, A. Swift heavy ion irradiation induced modifications in the optical band gap and Urbach's tail in polyaniline nanofibers. *Nucl. Instrum. Methods Phys. Res. Sect. B* **2011**, *269*, 2798. [CrossRef]

142. Ji, T.; Feng, Y.Y.; Qin, M.; Feng, W. Thermal conducting properties of aligned carbon nanotubes and their polymer composites. *Compos Part A Appl. Sci. Manuf.* **2016**, *91*, 351. [CrossRef]

143. Pocas, L.C.; Travain, S.A.; Duarte, J.L.; Silva, R.A.; Giacometti, J.A.; Marletta, A. Annealing effects on conductivity and optical properties of the PAni layer in ITO/PAni/PPV+DBS/Al polymer light-emitting diodes. *J. Phys. Condens. Matter.* **2007**, *19*, 436221. [CrossRef]

144. Dimitrov, S.D.; Schroeder, B.C.; Nielsen, C.B.; Bronstein, H.; Fei, Z.; McCulloch, I.; Heeney, M.; Durrant, J.R. Singlet Exciton Lifetimes in Conjugated Polymer Films for Organic Solar Cells. *Polymers* **2016**, *8*, 14. [CrossRef] [PubMed]

145. Scharber, M.C.; Mühlbacher, D.; Koppe, M.; Denk, P.; Waldauf, C.; Heeger, A.J.; Brabec, C.J. Design Rules for Donors in Bulk-Heterojunction Solar Cells—Towards 10% Energy-Conversion Efficiency. *Adv. Mater.* **2006**, *18*, 789–794. [CrossRef]